Immature myeloid cells directly contribute to skin tumor development by recruiting IL-17–producing CD4$^+$ T cells

Myrna L. Ortiz,[1]* Vinit Kumar,[2]* Anna Martner,[1,3]* Sridevi Mony,[2] Laxminarasimha Donthireddy,[2] Thomas Condamine,[2] John Seykora,[4] Stella C. Knight,[5] George Malietzis,[5,6] Gui Han Lee,[5,6] Morgan Moorghen,[6] Brianna Lenox,[1,3] Noreen Luetteke,[1] Esteban Celis,[7] and Dmitry Gabrilovich[2]

[1]H. Lee Moffitt Cancer Center and Research Institute, Tampa, FL 33612
[2]The Wistar Institute, Philadelphia, PA 19104
[3]Sahlgrenska Cancer Center, University of Gothenburg, S-405 30 Gothenburg, Sweden
[4]Department of Pathology and Laboratory Medicine, University of Pennsylvania, Philadelphia, PA 19104
[5]Antigen Presentation Research Group, Imperial College London, London HA1 3UJ, England, UK
[6]St. Mark's Hospital, Harrow HA1 3UJ, England, UK
[7]Cancer Immunology, Inflammation, and Tolerance Program, Georgia Regents University Cancer Center, Augusta, GA 30912

Evidence links chronic inflammation with cancer, but cellular mechanisms involved in this process remain unclear. We have demonstrated that in humans, inflammatory conditions that predispose to development of skin and colon tumors are associated with accumulation in tissues of CD33$^+$S100A9$^+$ cells, the phenotype typical for myeloid-derived suppressor cells in cancer or immature myeloid cells (IMCs) in tumor-free hosts. To identify the direct role of these cells in tumor development, we used S100A9 transgenic mice to create the conditions for topical accumulation of these cells in the skin in the absence of infection or tissue damage. These mice demonstrated accumulation of granulocytic IMCs in the skin upon topical application of 12-*O*-tetradecanoylphorbol-13-acetate (TPA), resulting in a dramatic increase in the formation of papillomas during epidermal carcinogenesis. The effect of IMCs on tumorigenesis was not associated with immune suppression, but with CCL4 (chemokine [C-C motif] ligand 4)-mediated recruitment of IL-17–producing CD4$^+$ T cells. This chemokine was released by activated IMCs. Elimination of CD4$^+$ T cells or blockade of CCL4 or IL-17 abrogated the increase in tumor formation caused by myeloid cells. Thus, this study implicates accumulation of IMCs as an initial step in facilitation of tumor formation, followed by the recruitment of CD4$^+$ T cells.

CORRESPONDENCE
Dmitry Gabrilovich:
dgabrilovich@wistar.org

Abbreviations used: BCC, basal cell carcinoma; DMBA, 7,12-dimethylbenz(a)anthracene; IHC, immunohistochemistry; IMC, immature myeloid cell; LC, Langerhans cell; MDSC, myeloid-derived suppressor cell; MΦ, macrophage; PMN, polymorphonuclear neutrophil; TPA, 12-*O*-tetradecanoylphorbol-13-acetate.

Inflammation develops in response to foreign agents or injuries and is crucial to the healing process. However, persistent unresolved inflammation can contribute to the development of cancer (Coussens et al., 2013). Despite the wealth of information implicating inflammation in tumor development, the specific role of different cells, especially myeloid cells, in this process remains largely unclear. Myeloid cells are an important component of inflammation. There is now ample evidence of abnormalities in the myeloid compartment in cancer, which manifests in inhibition of differentiation of DCs, polarization of macrophages (MΦs) toward M2 functional state, and dramatic expansion of myeloid-derived suppressor cells (MDSCs; Gabrilovich et al., 2012). MDSCs represent a heterogeneous population of pathologically activated myeloid cells that includes precursors of neutrophils (polymorphonuclear neutrophils [PMNs]), MΦs, DCs, and cells at earlier stages of myeloid cell differentiation (Gabrilovich and Nagaraj, 2009; Peranzoni et al., 2010; Youn et al., 2012). In mice, these cells are defined as Gr-1$^+$CD11b$^+$ cells with the

*M.L. Ortiz, V. Kumar, and A. Martner contributed equally to this paper.

The Rockefeller University Press $30.00
J. Exp. Med. 2015 Vol. 212 No. 3 351–367
www.jem.org/cgi/doi/10.1084/jem.20140835

recognition of polymorphonuclear (PMN-MDSC) and mononuclear (M-MDSC) subsets based on the expression of Ly6C and Ly6G markers (Fridlender et al., 2009; Peranzoni et al., 2010; Brandau et al., 2011; Youn et al., 2012). MDSCs are characterized by a potent immune-suppressive activity and the ability to promote tumor angiogenesis, tumor cell invasion, and metastases (Bierie and Moses, 2010; Gabrilovich et al., 2012; Talmadge and Gabrilovich, 2013). In tumor-free mice, cells with the same phenotype represent immature myeloid cells (IMCs) lacking immune-suppressive activity. Expansion of MDSCs is considered a consequence of tumor progression. However, in recent years, it has become clear that the cells with phenotypes and functions attributed to MDSCs are readily detectable in different conditions associated with chronic inflammation not directly linked to cancer (Cuenca et al., 2011; Nagaraj et al., 2013). We hypothesize that these cells can contribute to tumor development associated with inflammation. Understanding the role of specific components of inflammation in tumor development is difficult because of the fact that inflammation is a multicomponent complex process. To address this question, we focused on S100A9 protein. This is the member of the S100 family of Ca^{2+}-binding proteins with diverse biological activity, including chemotaxis of myeloid cells, fatty acid transport, production of reactive oxygen species, etc. (Markowitz and Carson, 2013). Expression of S100A9 together with its dimerization partner S100A8 is found predominantly in cells of the myeloid lineage. Differentiation of myelocytes/granulocytes is associated with an increase of S100A8/A9 expression, whereas differentiation of MΦs and DCs is associated with loss of their expression (Leder et al., 1990; Ehrchen et al., 2009; Srivastava et al., 2012; Markowitz and Carson, 2013). Cells of the lymphoid lineage do not express these proteins. We and others have previously found that accumulation of MDSCs and inhibition of DC differentiation in cancer were closely associated with up-regulation of S100A8/A9 (Cheng et al., 2008; Sinha et al., 2008; Ichikawa et al., 2011). The expansion of MDSCs was significantly reduced in S100A9-deficient mice treated with complete Freund's adjuvant or tumor-bearing mice (Cheng et al., 2008). In contrast, overexpression of S100A9 in mice resulted in accumulation of cells with MDSC phenotype (Chen et al., 2013). Furthermore, these data were consistent with a recent report that DCs derived from S100A9-deficient mice induced stronger response of allogeneic T cells (Shimizu et al., 2011). In recent years, S100A9 was identified as a marker of MDSCs in peripheral blood of cancer patients and tumor-bearing mice (Feng et al., 2012; Källberg et al., 2012; Zhao et al., 2012). We asked whether regulation of S100A9 level in myeloid cells could be used to dissect the possible role of MDSCs during early stages of tumor development. Here, we report that cells with the MDSC phenotype accumulate in tissues of patients with precancerous inflammation and that these cells play a major role in tumor development in mice. Importantly, this effect was not directly mediated by immune-suppressive mechanisms but by the recruitment of IL-17–producing $CD4^+$ T cells.

RESULTS

S100A9-positive myeloid cells in tissues of patients with inflammation or cancers

Although parameters for detection of MDSCs in peripheral blood of cancer patients by flow cytometry are well established, immunohistochemical detection of these cells in tissues has not been developed. Thus, we designed a double-staining protocol of tissues for the CD33 myeloid marker and S100A9 using confocal microscopy (Fig. 1 A). S100A9 was used for MDSC detection because this protein is directly implicated in accumulation of these cells in cancer and is shown as an MDSC marker in peripheral blood of cancer patients. The presence of $CD33^+S100A9^+$ was then assessed in skin of patients with melanoma and basal cell carcinoma (BCC), as well as in patients with several inflammatory skin diseases (Fig. 1 B). No increase in the presence of these cells was found in patients with lichen planus or psoriasis as compared with controls. In contrast, patients with spongiotic dermatitis (eczema) had significantly ($P = 0.001$) higher numbers of $CD33^+$ $S100A9^+$ cells in skin. The presence of these cells was a little higher in patients with BCC. Patients with melanoma had a dramatic increase in number of these cells (Fig. 1 C). $CD33^+$ $S100A9^+$ cells can represent not only IMCs or MDSCs but also PMNs because the expression of S100A9 is retained in these cells as opposed to MΦs or DCs (Leder et al., 1990; Ehrchen et al., 2009; Srivastava et al., 2012; Markowitz and Carson, 2013). Therefore, we evaluated the presence of PMNs in skin using a specific marker neutrophil elastase. No difference in the number of PMNs was found for any of the conditions except in patients with melanoma (Fig. 1 C). $CD163^+$ MΦs were modestly increased in skin of patients with eczema, BCC, and melanoma (Fig. 1 C). We also evaluated colon tissue samples from a cohort of patients with ulcerative colitis with evidence of dysplasia and colon from cancer patients. Dramatic (>10-fold) increase in the presence of $CD33^+S100A9^+$ cells was found in tissues from patients with colitis and colon cancer, whereas the number of PMNs and MΦs increased less than twofold (Fig. 1 E). Lichen planus and psoriasis are not associated with the development of skin cancer, whereas history of eczema is an independent predictor of BCC (Dyer et al., 2012). Ulcerative colitis, especially in patients with dysplasia, is associated with colon cancer (Dalgleish and O'Byrne, 2006; Dyson and Rutter, 2012). These results indicate that the population of $CD33^+S100A9^+$ cells represented by IMCs or MDSCs is dramatically increased in select inflammatory conditions, which are associated with an increased risk for developing cancer.

The role of IMCs in tumor development

Next we asked what role, if any, these cells can play in tumor development. To address this question, we used mice with overexpression of S100A9 protein in hematopoietic cells (S100A9Tg mice; Cheng et al., 2008). S100A9Tg mice (FVB/N background) had no detectable abnormalities during the first months of life (Chen et al., 2013). Compared with WT mice, S100A9Tg mice expressed higher amounts of S100A9 protein

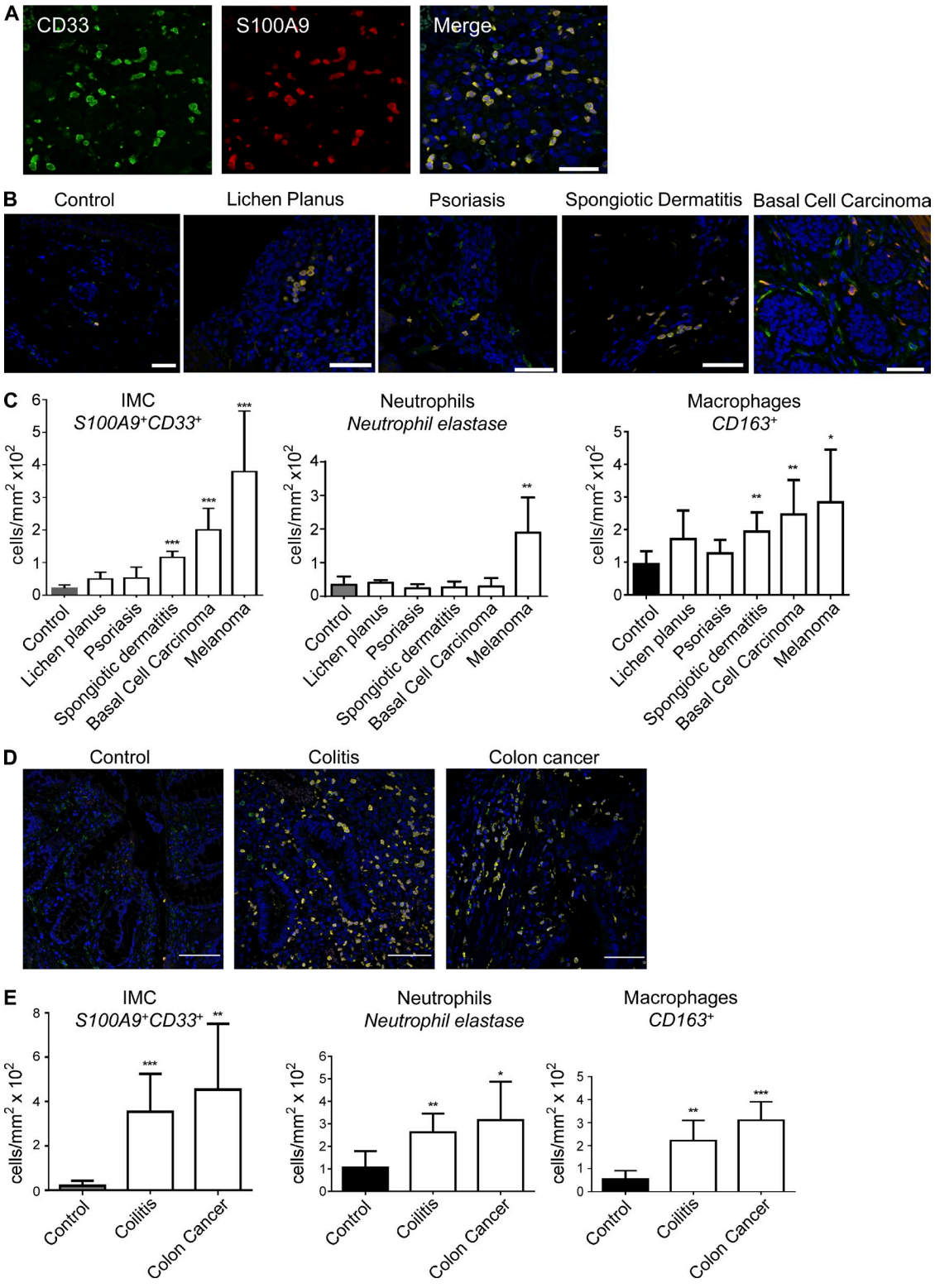

Figure 1. Myeloid cells in human tissues. (A) Example of staining of melanoma with CD33 and S100A9 antibody. (B) Typical example of staining of tissues from patients with different skin pathologies. (C) The number of different myeloid cells in skin. Each group included five patients. (D) Typical example of staining of tissues from patients with colitis and colon cancer. (A, B, and D) Bars, 50 µm. (E) The number of different myeloid cells in colonic tissues. Control and colon cancer groups included six patients and colitis group included five patients. (C and E) Mean and SD are shown. The differences from control: *, $P < 0.05$; **, $P < 0.01$; ***, $P < 0.001$.

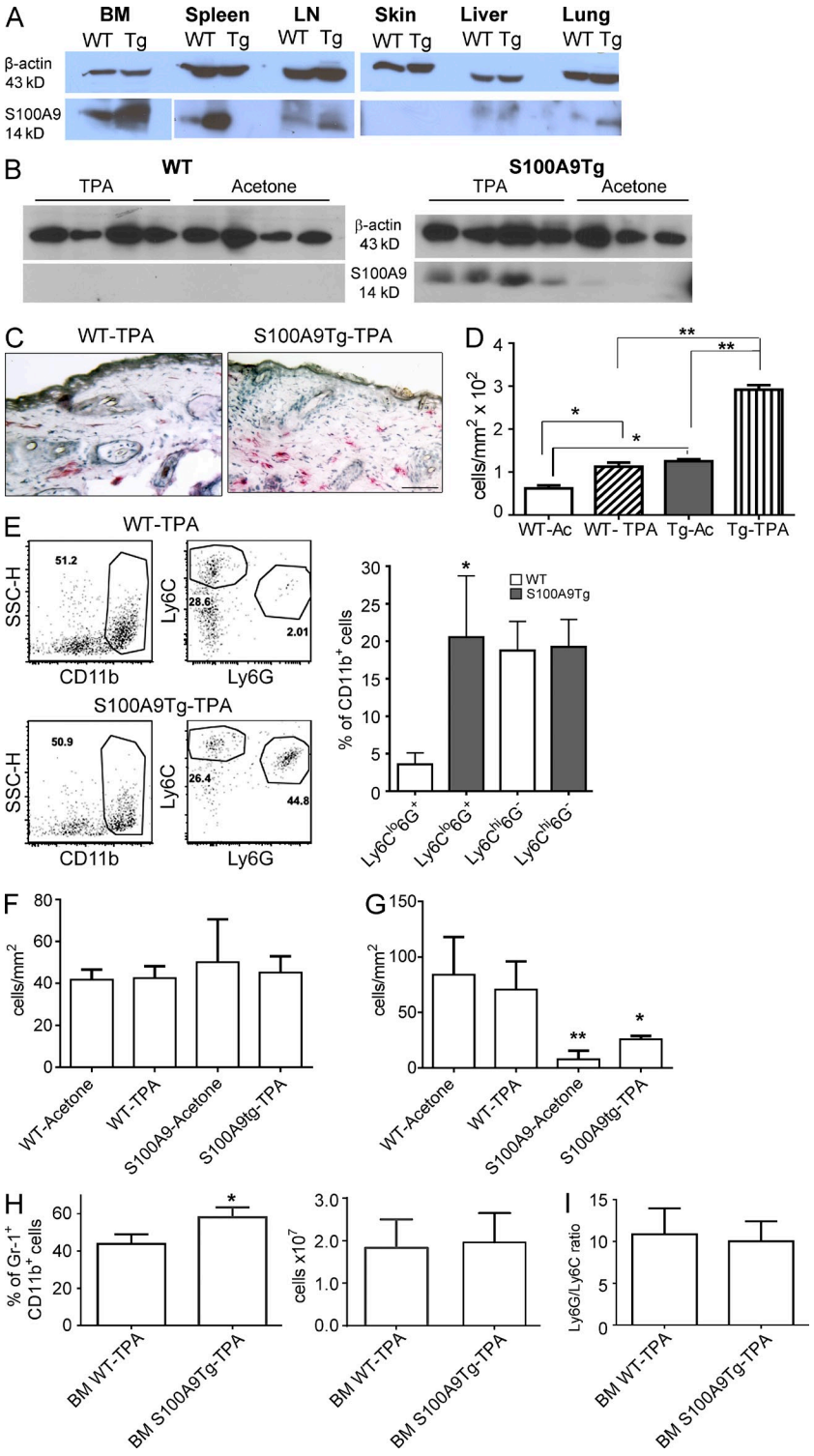

Figure 2. Accumulation of IMCs in skin of S100A9Tg mice. (A) Amount of S100A9 protein in various organs of WT and S100A9Tg mice. Typical example of Western blotting of 30 µg tissue protein is shown. (B) S100A9 protein in skin samples from WT and S100A9Tg mice treated with TPA or vehicle (acetone). Each lane represents an individual mouse. (C) Representative IHC images showing the presence of Gr-1+ cells in skin. Bar, 100 µm. (D) The number of Gr-1+ cells per square millimeter of skin tissue. (E) Phenotype of myeloid cells accumulated in skin of TPA-treated mice. Representative flow cytometry plots are shown with numbers indicating percentage of gated cells. Bar graph on the right illustrates the proportions of cell populations. (F and G) The number of F4/80+ (F) and CD11c+ (G) cells in skin of mice treated with TPA or acetone as indicated. (H and I) Proportion (left) and absolute number (right) of Gr-1+CD11b+ (H) and Ly6C/Ly6G ratio within the population of CD11b+ cells (I) in BM of TPA-treated mice. (D–I) Each group included four mice. Mean and SD are shown. *, $P < 0.05$; **, $P < 0.01$.

in BM, spleen, LNs, and lung, but not in skin or liver (Fig. 2 A). Two models of skin carcinogenesis were used. Tg.AC mice (also FVB/N) express the mutant *v-h-ras* transgene under the ζ-globin promoter. When treated topically with the tumor promoter 12-*O*-tetradecanoylphorbol-13-acetate (TPA), Tg.AC mice develop multiple papillomas, some of which progress to a malignant stage (Humble et al., 2005). In C57BL/6 mice, skin tumor formation was induced by a single application of the carcinogen 7,12-dimethylbenz(a)anthracene (DMBA), followed by 12-wk topical treatment with TPA.

Topical treatment of WT mice with TPA for 4 wk did not result in detectable levels of S100A9 in skin. In contrast,

untreated S100A9Tg mice had a low level of the protein, and TPA treatment of S100A9Tg mice caused a substantial increase in the amount of the protein (Fig. 2 B). Although treatment of WT mice with TPA resulted in only a small increase in the number of Gr-1$^+$ cells in skin (evaluated by immunohistochemistry [IHC]), in S100A9Tg mice these cells increased approximately threefold ($P < 0.01$; Fig. 2, C and D). Evaluation of cells derived from skin sample digests by flow cytometry revealed that all the Gr-1$^+$ cells also expressed CD11b and thus have phenotypic markers of MDSCs. The proportion of Ly6C^{hi}Ly6G$^-$ monocytic cells among CD11b$^+$ cells in TPA-treated skin was the same in WT and S100A9Tg mice, whereas the proportion of Ly6C^{lo}Ly6G$^+$ granulocytic cells was significantly higher in S100A9Tg than in WT mice (Fig. 2 E). No differences in the numbers of F4/80$^+$ MΦs between WT and S100A9Tg skin were found (Fig. 2 F), whereas the number of CD11c$^+$ skin DCs was significantly lower in both acetone- and TPA-treated S100A9Tg than in WT mice (Fig. 2 G). We investigated whether the dramatic increase of granulocytic cells in the skin of S100A9Tg mice was the result of their expansion in BM. There was a slight increase in the presence of these cells in BM of TPA-treated S100A9Tg versus WT mice, but the ratio between granulocytic and monocytic subsets of IMCs was the same (Fig. 2, H and I). These data indicate that, consistent with previous observations (Cheng et al., 2008), the overexpression of S100A9 in myeloid progenitors did not cause expansion of myeloid cells but rather diverted their differentiation toward immature granulocytic cells. As a result, topical application of TPA in S100A9Tg mice caused substantial accumulation of IMCs with granulocytic phenotype, whereas the presence of MΦs and DCs was either unchanged or decreased.

To study skin carcinogenesis, the S100A9Tg mice were crossed with homozygous Tg.AC mice, and hemizygous monotransgenic (Tg.AC) and bitransgenic (S100A9; Tg.AC) littermates were topically treated twice weekly for 6 wk with the tumor promoter TPA. Papillomas developed much faster and at significantly ($P < 0.001$) higher numbers in bitransgenic mice expressing S100A9Tg than in monotransgenic mice (Fig. 3 A). S100A9 expression could be induced in keratinocytes under inflammatory conditions (Sorenson et al., 2012). To clarify the role of infiltrating BM-derived cells in increased tumorigenesis in S100A9Tg mice, lethally irradiated Tg.AC mice were reconstituted with BM from WT or S100A9Tg mice, and papilloma formation was similarly evaluated after TPA treatment. Recipients of S100ATg BM developed significantly ($P < 0.05$) more papillomas than recipients of BM from WT mice (Fig. 3 B), demonstrating that up-regulation of S100A9 in BM-derived hematopoietic cells was responsible for increased tumor formation. To confirm a specific role of IMCs in tumor development, Gr-1$^+$ cells were depleted in Tg.AC mice with Gr-1 antibody during the first 3 wk of TPA treatment. This treatment significantly ($P < 0.05$) reduced papilloma formation (Fig. 3 C). To evaluate the direct effect of accumulation of IMCs on proliferation of keratinocytes, WT and S100A9Tg mice were treated

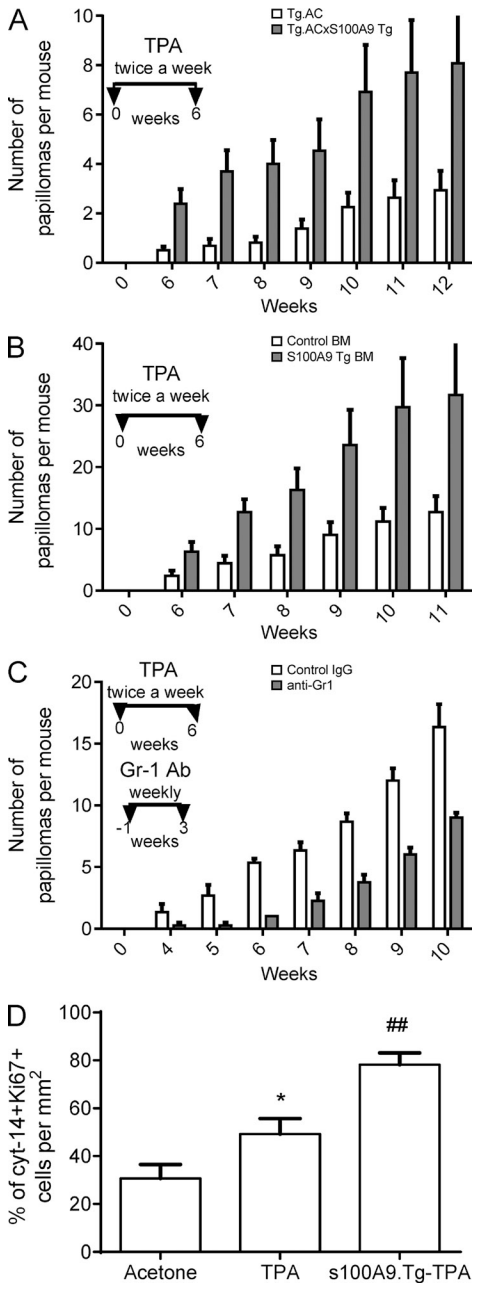

Figure 3. IMCs enhance papilloma formation. (A) Papilloma development in Tg.AC and S100A9Tg;Tg.AC bitransgenic mice after TPA treatment for 6 wk. Each group included seven mice. Two-way ANOVA, $P = 0.0071$. (B) Papilloma development in lethally irradiated Tg.AC mice that received BM from S100A9Tg or WT (control) mice. TPA treatment started 3 wk after the BM transfer. Each group included four mice. Two-way ANOVA, $P = 0.035$. (C) Papilloma development in S100A9Tg;Tg.AC mice treated with Gr-1 antibody and TPA as indicated in the graph. Each group included five mice. Two-way ANOVA, $P < 0.001$. (A and C) Mean and SD of the number of papillomas per mouse are shown. (D) Proliferation of keratinocytes in WT and S100A9Tg FVB/n mice treated for 5 wk with TPA. The proportion of proliferating Ki67$^+$ cells among all cytokeratin 14$^+$ keratinocytes was calculated in at least 100 cells. Each group included three mice. *, $P < 0.05$ between TPA- and acetone-treated WT mice; ##, $P < 0.01$ between TPA-treated WT and S100A9Tg mice. (B and D) Mean and SD are shown.

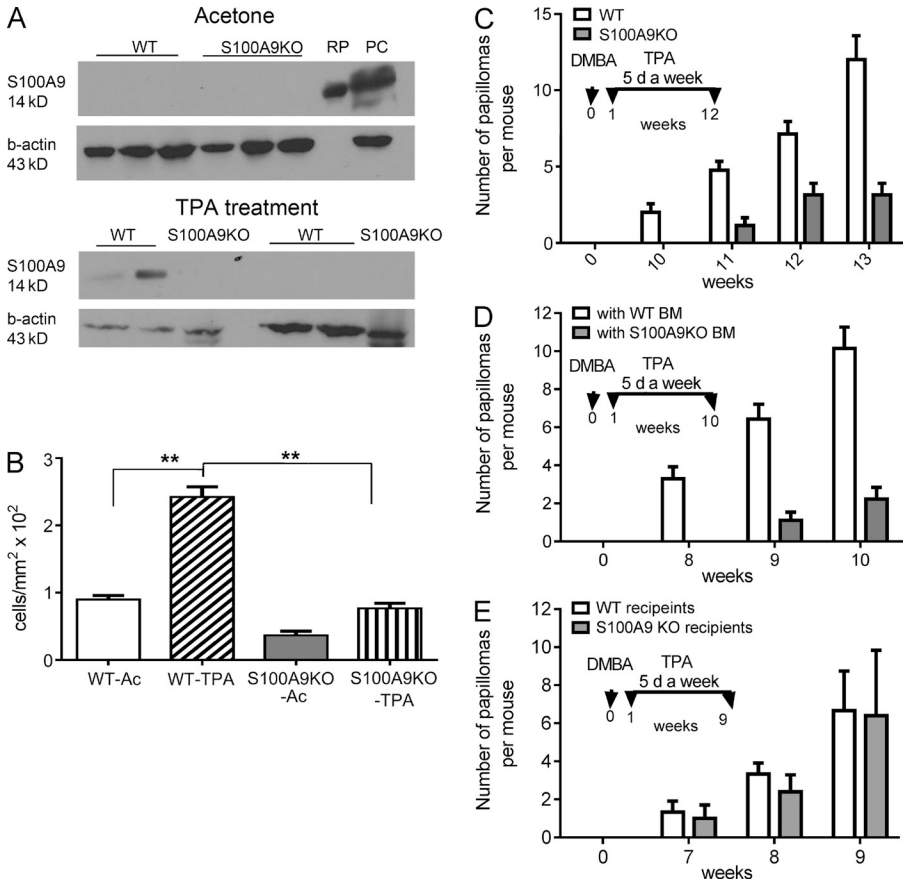

Figure 4. Lack of IMCs prevents tumor formation. (A) S100A9 protein in skin of C57BL/6 WT and S100A9KO mice treated with TPA or acetone vehicle. Each lane represents an individual mouse. Splenocytes from a tumor-bearing mouse were used as a positive control (PC). RP, recombinant protein. (B) The number of Gr-1$^+$ cells in skin of C57BL/6 mice evaluated by IHC. Mice were treated with TPA or acetone for 4 wk. Each group included four mice. **, $P < 0.01$. (C) The number of papillomas in WT and S100A9KO C57BL/6 mice induced by DMBA and TPA as indicated. Each group included seven mice. $P = 0.003$. (D) Number of papillomas in lethally irradiated C57BL/6 mice that received BM from S100A9KO or WT (control) mice. Carcinogen treatment initiated 3 wk after the BM transfer. Each group included four mice. $P < 0.001$. (E) Number of papillomas in lethally irradiated C57BL/6 WT or S100A9KO mice that received BM from WT mice. Carcinogen treatment initiated 4 wk after the BM transfer. Each group included four mice ($P > 0.1$). (B–E) Mean and SD are shown.

with TPA for 5 wk, and the proportion of proliferating keratinocytes (cytokeratin 14$^+$Ki67$^+$ cells) was evaluated. TPA treatment caused proliferation of keratinocytes in WT mice, which was significantly ($P < 0.01$) enhanced in S100A9Tg mice (Fig. 3 D).

To better ascertain the possible role of IMCs in tumor development, we also used mice with targeted deletion of S100A9 (S100A9KO mice, C57BL/6 background; Manitz et al., 2003). In contrast to FVB/N mice, untreated WT C57BL/6 mice had traces of S100A9 protein in the skin, which was increased after 4 wk of TPA treatment (Fig. 4 A). S100A9KO mice had no detectable S100A9 protein in the skin (Fig. 4 A). Treatment of WT C57BL/6 mice with TPA greatly increased the number of Gr-1$^+$ myeloid cells in the skin, whereas in S100A9KO mice, this increase was very modest and lower than in WT mice (Fig. 4 B). In contrast to S100A9Tg mice, S100A9KO mice developed significantly ($P < 0.01$) fewer skin tumors than their WT C57BL/6 counterparts after treatment with both DMBA and TPA (Fig. 4 C). Furthermore, mice reconstituted with BM from S100A9KO mice had significantly ($P < 0.01$) fewer lesions than mice reconstituted with WT BM (Fig. 4 D), confirming the critical role of BM-derived cells in modulating skin tumorigenesis. To further verify a specific role of BM-derived cells in tumor development, WT and S100A9 KO mice were reconstituted with BM from WT mice. No differences were found in the numbers of papillomas between WT and S100A9KO mice recipients treated with DMBA followed by TPA (Fig. 4 E). Collectively, these data demonstrate that development of skin tumors directly depends on the accumulation of granulocytic IMCs in the skin. Next we investigated the mechanism or mechanisms by which IMCs mediated tumor promotion.

Accumulation of IMCs in skin did not result in immune suppression

We tested the hypothesis that IMCs accumulated in TPA-treated S100A9Tg skin had immune-suppressive activity and thus could be defined as MDSCs. S100A9Tg mice were backcrossed for nine generations to C57BL/6 mice. Mice were treated for 6 wk with topical application of TPA. Ly6G$^+$ granulocytic IMCs were isolated from the skin and were co-cultured with splenocytes from OT-1 mice stimulated with control or specific peptides. In contrast to the cells with the same phenotype isolated from spleens of tumor-bearing mice (MDSCs), skin-infiltrating granulocytic cells from TPA-treated mice did not suppress antigen-specific T cell response (Fig. 5 A). Similarly, Gr-1$^+$CD11b$^+$ cells isolated from BM of WT and S100A9Tg mice treated with TPA also lacked immune-suppressive activity (Fig. 5 B). In contrast, cells with the same phenotype isolated from BM of tumor-bearing mice (MDSCs) demonstrated profound suppressive

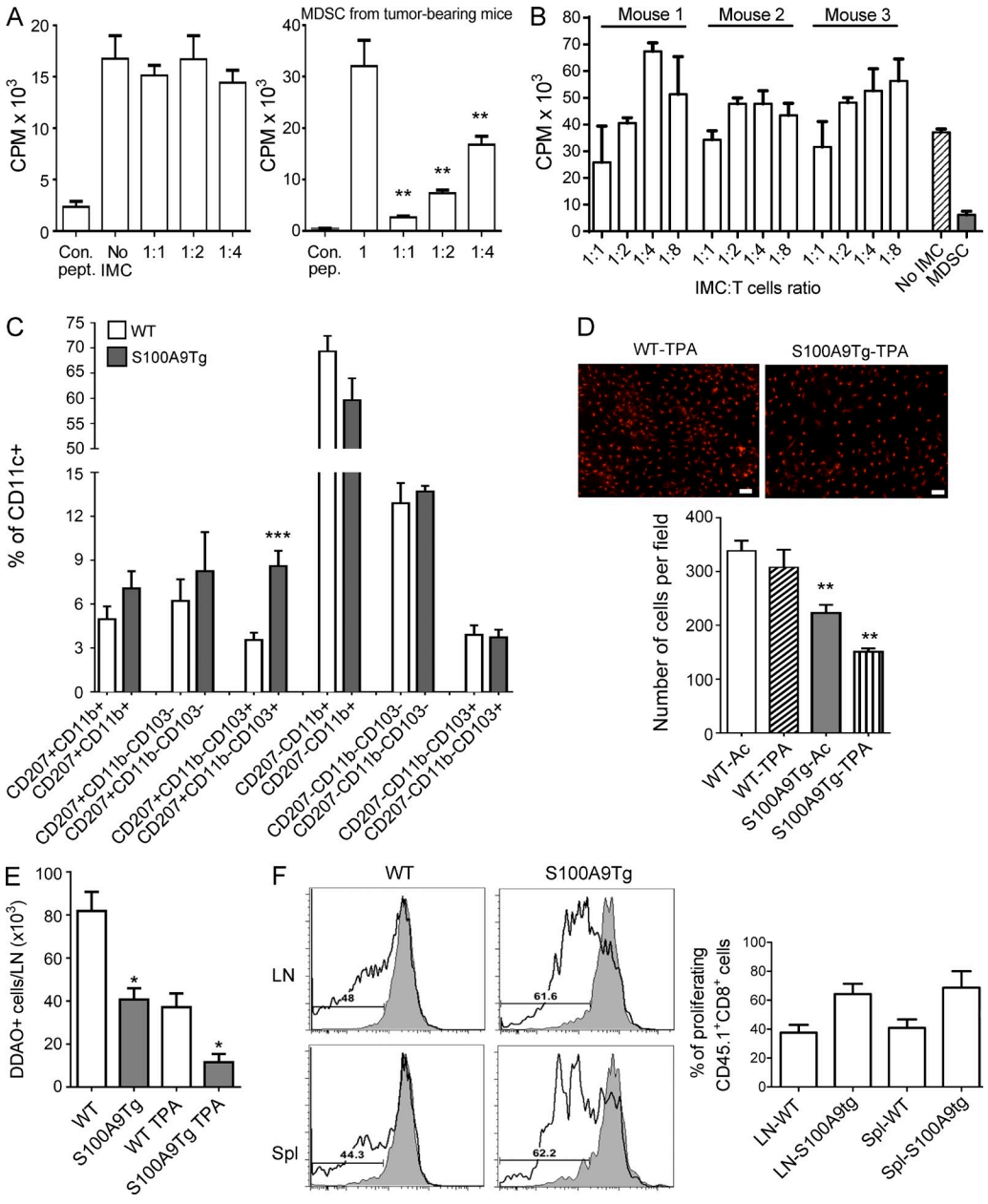

Figure 5. IMCs lack suppressive activity. (A) Suppressive activity of Gr-1$^+$ cells isolated from skin of S100A9Tg C57BL/6 mice treated for 6 wk with TPA. IMCs were added to splenocytes from OT-1 mice at the indicated ratios. Cells were incubated for 3 d in the presence of specific (SIINFEKL) or control (gp100) peptide. Proliferation was measured in triplicates by [^{3}H]thymidine incorporation. Each experiment included three mice. (right) Antigen-specific suppressive assay with Gr-1$^+$ MDSCs isolated from spleens of EL-4 tumor-bearing mice. Mean and SD are shown. **, $P < 0.01$ from no MDSC control. (B) Suppression activity of Gr-1$^+$CD11b$^+$ IMCs isolated from BM of mice treated with TPA. Allogeneic mixed lymphocyte reactions were performed using CD3-depleted irradiated FVB/N splenocytes as stimulators and BALB/c T cells as responders, mixed at 1:1 ratio. IMCs were added to the mix at the indicated ratios. Proliferation was measured in triplicates by [^{3}H]thymidine incorporation ($n = 3$). Mean and SD are shown. (C) The phenotype of DCs isolated from skin of TPA-treated WT and S100A9Tg mice. Each group included four mice. Mean and SD are shown. ***, $P < 0.001$. (D) LCs in epidermis of mice. (top) Representative image of LCs. Bars, 50 µm. (bottom) Bar graph shows cumulative result of the number of LCs per 1 mm^2 of epidermis. Each group included four mice (mean and SD are shown). **, $P < 0.01$. (E) Migration of skin DCs to draining LNs. Dorsal shaved skins of WT and S100A9Tg mice previously treated with acetone or TPA were painted with DDAO, and 24 h later DDAO$^+$CD11c$^+$ cells were evaluated in draining LNs by flow cytometry. Each experiment was performed three times. Mean and SD are shown. *, $P < 0.05$. (F) T cells from OT1 mice were labeled with DDAO fluorescent dye and injected i.v. into TPA-treated WT and S100A9Tg C57BL/6 mice. OVA was applied to the skin 24 h later, and LNs and CD8$^+$CD45.1$^+$ T cell spleens were evaluated by flow cytometry 3 d after the application. A typical example of the CD8$^+$CD45.1$^+$ T cell proliferation is shown on the left, and cumulative results (mean ± SD) of three mice in each group are shown on the right.

activity (Fig. 5 B). Because S100A9Tg mice had reduced presence of $CD11c^+$ DCs in the skin as compared with WT mice, we analyzed in more detail the different populations of DCs in skin by flow cytometry. Only slight differences between WT and S100A9Tg mice were seen in the proportion of subsets of skin DCs (Fig. 5 C), with the exception of $CD207^+CD11b^-CD103^+$ DCs, which were significantly elevated in S100A9Tg mice compared with WT mice (Fig. 5 C). S100A9Tg had a modestly ($P < 0.01$) reduced number of Langerhans cells (LCs) in epidermis (Fig. 5 D). To determine whether those changes would translate into decreased migration of DCs to draining LNs, WT and S100A9Tg mice were treated topically with acetone vehicle or TPA for 4 wk, after which the skin was painted with fluorescent dye DDAO. The next day, skin-draining LNs were collected and $DDAO^+$ DCs were counted. We found significantly lower numbers of $DDAO^+CD86^+IA^{bright}$ migratory DCs in LNs of S100A9Tg mice than in WT mice (Fig. 5 E).

We wondered whether reduction in DC numbers and migration in S100A9Tg skin could result in impaired priming of $CD8^+$ T cells. DDAO-labeled OVA-specific OT-1 T cells were transferred to WT or S100A9Tg C57BL/6 mice pretreated for 4 wk with TPA. OVA protein was applied to the same part of the skin as TPA, and 3 d later, proliferation of OT-1 T cells was evaluated in LNs and spleen. Robust proliferation of OT-1 cells was observed in all mice. No differences were found between WT and S100A9Tg mice (Fig. 5 F). These results indicate that despite reduced presence of DCs in the skin, antigen-specific response was unaffected in S100A9Tg mice. Together with the data indicating lack of immune-suppressive activity of IMCs, this finding suggests that immune suppression is not the primary reason for increased tumor formation in S100A9Tg mice.

IMCs recruit $CD4^+$ T cells to the skin

We evaluated the presence of lymphocytes in the skin of vehicle- and TPA-treated mice. No significant differences between WT and S100A9Tg mice were found in the presence of B lymphocytes, NK cells, or $CD8^+$ T cells (not depicted). In contrast, treatment with TPA resulted in the marked accumulation of $CD4^+$ T cells in the skin that was significantly ($P < 0.01$) higher in S100A9Tg mice than in WT mice (Fig. 6 A). A small statistically nonsignificant increase was observed in the population of γδ T cells (Fig. 6 B). Conversely, in S100A9KO mice, TPA only caused a modest increase in skin $CD4^+$ T cells as compared with the prominent accumulation observed in WT C57BL/6 mice (Fig. 6 C). Skin $CD8^+$ T cells in both WT and S100A9KO mice were comparably low and unaffected by TPA treatment (not depicted).

The characteristics of $CD4^+$ T cells in skin of TPA-treated mice were studied using flow cytometry. Consistent with the data obtained by IHC, the proportion of $CD4^+$ T cells among hematopoietic $CD45^+$ cells in skin was significantly ($P < 0.001$) higher in S100A9Tg mice than in WT mice (Fig. 6 D). The prevalence of different subsets within the population of $CD4^+$ T cells in skin was measured using intracellular cytokine staining. No substantial differences were found between WT and S100A9Tg mice in the proportion of most $CD4^+$ T cell populations. However, S100A9Tg skin showed higher proportions of $IL\text{-}22^+$ and $IL\text{-}10^+$ cells and $FoxP3^+CD4^+$ T reg cells and a significantly lower proportion of $IL\text{-}13^+CD4^+$ cells than WT skin (Fig. 6 E). No differences were seen between WT and S100A9Tg skin treated with acetone vehicle alone (not depicted). It was possible that although the proportion of cytokine-producing $CD4^+$ T cells was not changed, the level of cytokine production on a per cell basis could be different. However, no differences were found in the fluorescence intensity of those cytokines that showed no changes in the proportion of cells (not depicted). To investigate the ability of IMCs to directly polarize $CD4^+$ T cells in vitro, naive $CD4^+CD62L^+$ T cells were co-cultured with IMCs isolated from BM of TPA-treated WT or S100A9Tg mice. No evidence of $CD4^+$ T cell polarization was found (Fig. 6 F). Thus, accumulation of IMCs in skin of S100A9Tg mice was associated with substantial increase in the presence $CD4^+$ T cells. $Gr\text{-}1^+$ IMCs and $CD4^+$ T cells localized in the same vicinity in dermis of TPA-treated mice. In contrast, γδ T cells resided in the different area of the skin (close to epidermis; Fig. 6 G). We proposed that although IMCs did not cause specific polarization of $CD4^+$ T cells, they could recruit a substantial proportion of proinflammatory T cell populations. This hypothesis was tested in further experiments.

We investigated whether enhanced tumor formation in S100A9Tg mice was mediated by $CD4^+$ T cells. S100A9Tg;Tg. AC bitransgenic mice were treated with control IgG- or CD4-specific antibody before and during the first 3 wk of TPA application. CD4 antibody significantly ($P < 0.01$) reduced the formation of papillomas in these mice (Fig. 7 A), indicating that the tumor-promoting effect of IMCs is mediated via recruitment of $CD4^+$ T cells. We asked whether depletion of $CD4^+$ T cells could affect TPA-inducible accumulation of IMCs in skin. To address this question, the presence of $CD4^+$ T cells and $Gr\text{-}1^+$ IMCs was evaluated in skin of mice treated with TPA and CD4 antibody for 5 wk. This treatment resulted in abrogation of $CD4^+$ T cell accumulation but did not affect $Gr\text{-}1^+$ cells (Fig. 7 B).

Because IMCs attracted a large number of $CD4^+$ to the skin, even without causing preferential recruitment of T cell populations, the total number of proinflammatory $CD4^+$ T cells in the skin would substantially increase. We asked whether the levels of cytokines produced by $CD4^+$ T cells were different in skin of S100A9Tg and WT mice. The cytokines were also measured in spleen and BM, where no significant changes in myeloid or lymphoid cells were observed. No differences were found in the amount of IL-10 or IL-22 between TPA-treated WT and S100A9Tg mice. In contrast, the amount of IL-17A was significantly higher in the skin but not spleen and BM of S100A9Tg mice than in WT mice (Fig. 7 C). $CD4^+$ T cells appear to play a major role in IL-17A accumulation in skin because depletion of $CD4^+$ T cells abrogated TPA-inducible increase in IL-17A in

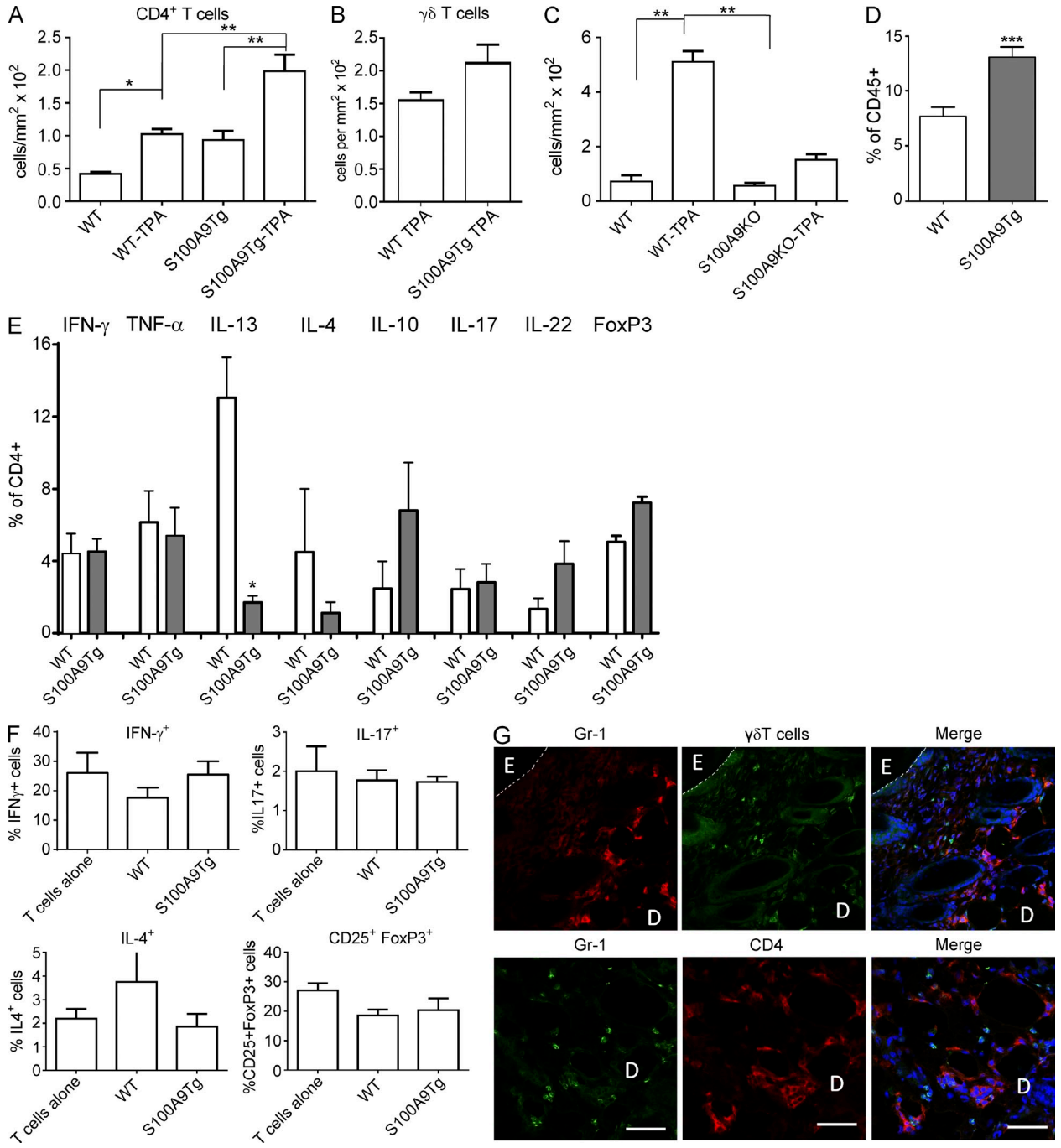

Figure 6. IMCs recruit CD4+ T cells to the skin. (A) The number of CD4+ T cells in the skin of WT and S100A9Tg FVB/N mice. The number of cells was evaluated by IHC and counted per square millimeter of tissue. Each experiment included five mice. (B) The number of γδ T cells in skin of TPA-treated WT and S100A9Tg C57BL/6 mice. The number of cells was evaluated by IHC and counted per square millimeter of tissue ($n = 3$). (C) The number of CD4+ T cells in the skin of WT and S100A9KO C57BL/6 mice evaluated by IHC and counted per square millimeter of tissue. Each experiment included five mice. (D) The proportion of CD4+ cells among CD45+ hematopoietic cells in WT and S100A9Tg mice treated with TPA and evaluated by flow cytometry. Six mice per group. (E) Intracellular staining of different cytokines in cells isolated from the skin of WT and S100A9Tg mice treated with TPA. CD4+ cells were gated. Each group included three to six mice. (F) Polarization of naive CD62L+CD4+ T cells by IMCs in vitro. T cells were cultured with BM IMCs from WT and S100A9Tg mice at a 1:1 ratio for 4 d in the presence of CD3/CD28 beads. Cells were then stimulated for 4 h with TPA/ionomycin in the presence of GolgiStop. Intracellular cytokines were evaluated within the population of CD4+ T cells by flow cytometry ($n = 5$). (A–F) Mean and SD are shown. *, $P < 0.05$; **, $P < 0.01$; ***, $P < 0.001$. (G) Localization of Gr-1+ and CD4+ T cells or γδ T cells in skin of TPA-treated S100A9Tg mice. Immunofluorescent microscopy with the indicated antibodies is performed. Merge staining included DAPI (blue). Typical example of three experiments is shown. Epidermis and dermis are marked with E and D. Please note that to see accumulated CD4+ T cells in the skin, the field had to be moved further down and epidermis was outside the area. Bars, 50 µm.

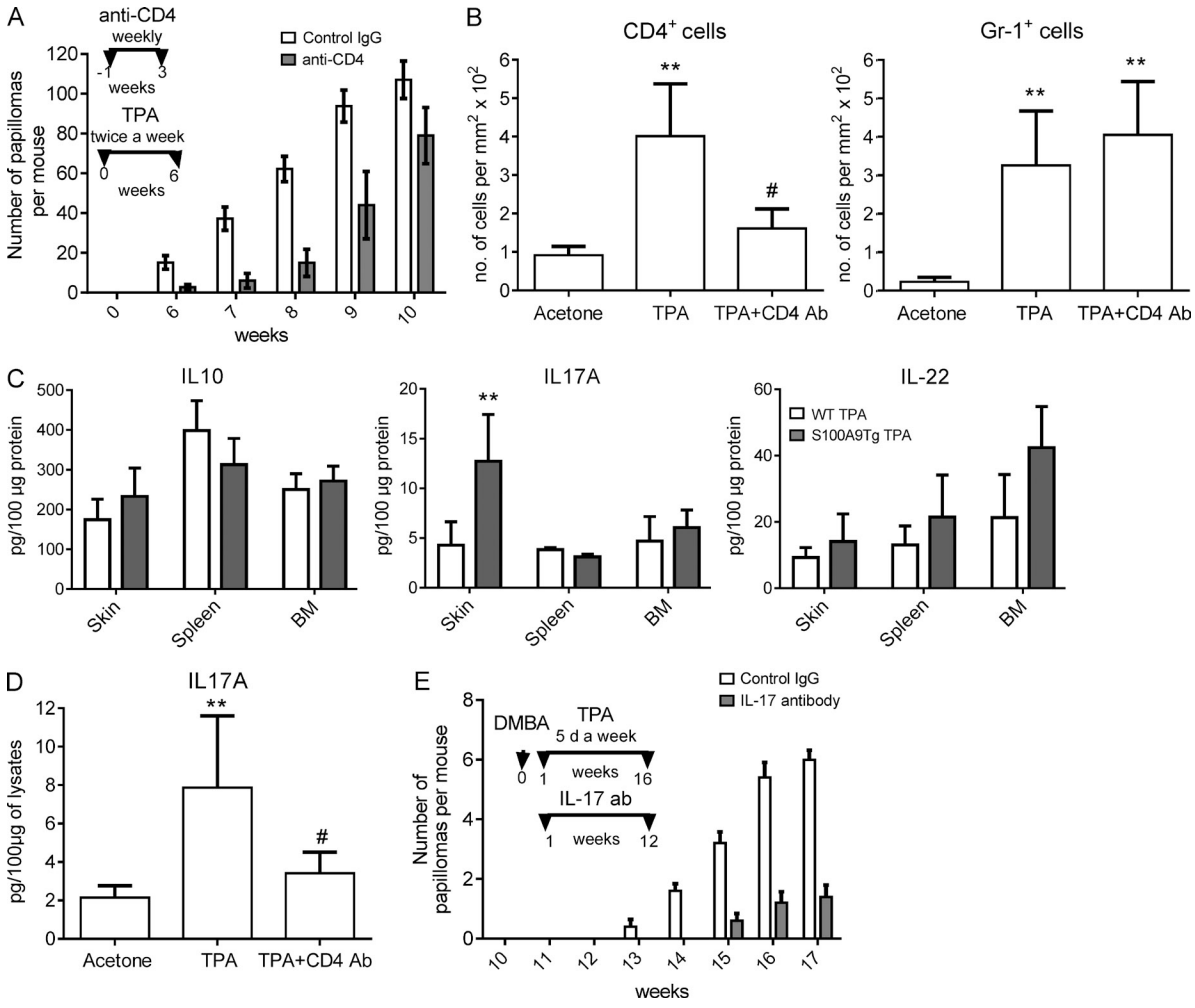

Figure 7. The role of IL-17 in IMC-mediated enhancement of papilloma formation. (A) Papilloma development in CD4-depleted S100A9Tg;Tg.AC bitransgenic mice. CD4 antibody or IgG (control) treatment was performed as indicated on the graph. Mean and SD of papillomas per mouse are shown. Each group included five mice. Two-way ANOVA, P = 0.021. (B) The presence of CD4+ T cells and Gr-1+ IMCs in skin of C57BL/6 S100A9Tg mice treated with TPA and CD4 antibody for 5 wk. Cells were evaluated by IHC ($n = 4$). (C) The presence of cytokines in tissues of WT and S100A9Tg mice treated with TPA for 6 wk. Cytokines were measured in whole cell lysates using ELISA. **, P < 0.01. (D) The amount of IL-17A in skin of mice described in B measured by ELISA. (B and D) **, P < 0.01 from acetone-treated mice; #, P < 0.05 from TPA only–treated mice ($n = 6$). (E) Papilloma formation in S100A9Tg C57BL/6 mice was induced by DMBA application, followed by 16 wk of treatment with TPA. Mice were treated with 200 µg of either control IgG or neutralizing IL-17 antibody during the first 12 wk. Each group included five mice. Two-way ANOVA, P < 0.001. (B–E) Mean and SD are shown.

the skin (Fig. 7 D). These data suggested that IL-17 could play an important role in IMC-mediated promotion of tumor formation. To test this hypothesis, we used IL-17 neutralizing antibody in C57BL/6 S100A9Tg and WT mice treated with DMBA and TPA. Blockade of IL-17 dramatically reduced papilloma formation in S100A9Tg mice (Fig. 7 E). Thus, accumulation of granulocytic IMCs in skin resulted in recruitment of CD4+ T cells and to a lesser extent γδ T cells that could promote tumor development via release of IL-17.

The mechanism of IMC-inducible recruitment of CD4+ T cells

How could IMCs recruit CD4+ T cells? We evaluated the ability of IMCs to attract CD4+ cells in vitro. Supernatants from normal BM-derived IMCs had no effect on CD4+ T cell migration. However, IMCs activated with LPS or TPA secreted potent chemotactic activity for CD4+ T cells (Fig. 8 A and not depicted). Importantly, chemotaxis of CD4+ T cells was observed only if T cells were also stimulated before the assay (Fig. 8 A). When IMC supernatants were placed in both chambers during the assay, CD4+ T cell migration was significantly reduced, indicating that the effect was indeed the result of chemotaxis (not depicted).

Using RNA isolated from skin, we examined expression of chemokines known to be involved in the migration of CD4+ T cells. Expression of *ccl3* (*chemokine [C-C motif] ligand 3*) and *ccl4* RNAs was significantly (P < 0.05) up-regulated in the skin of TPA-treated S100A9Tg mice compared with WT mice, whereas the expression of *ccl22* was modestly increased

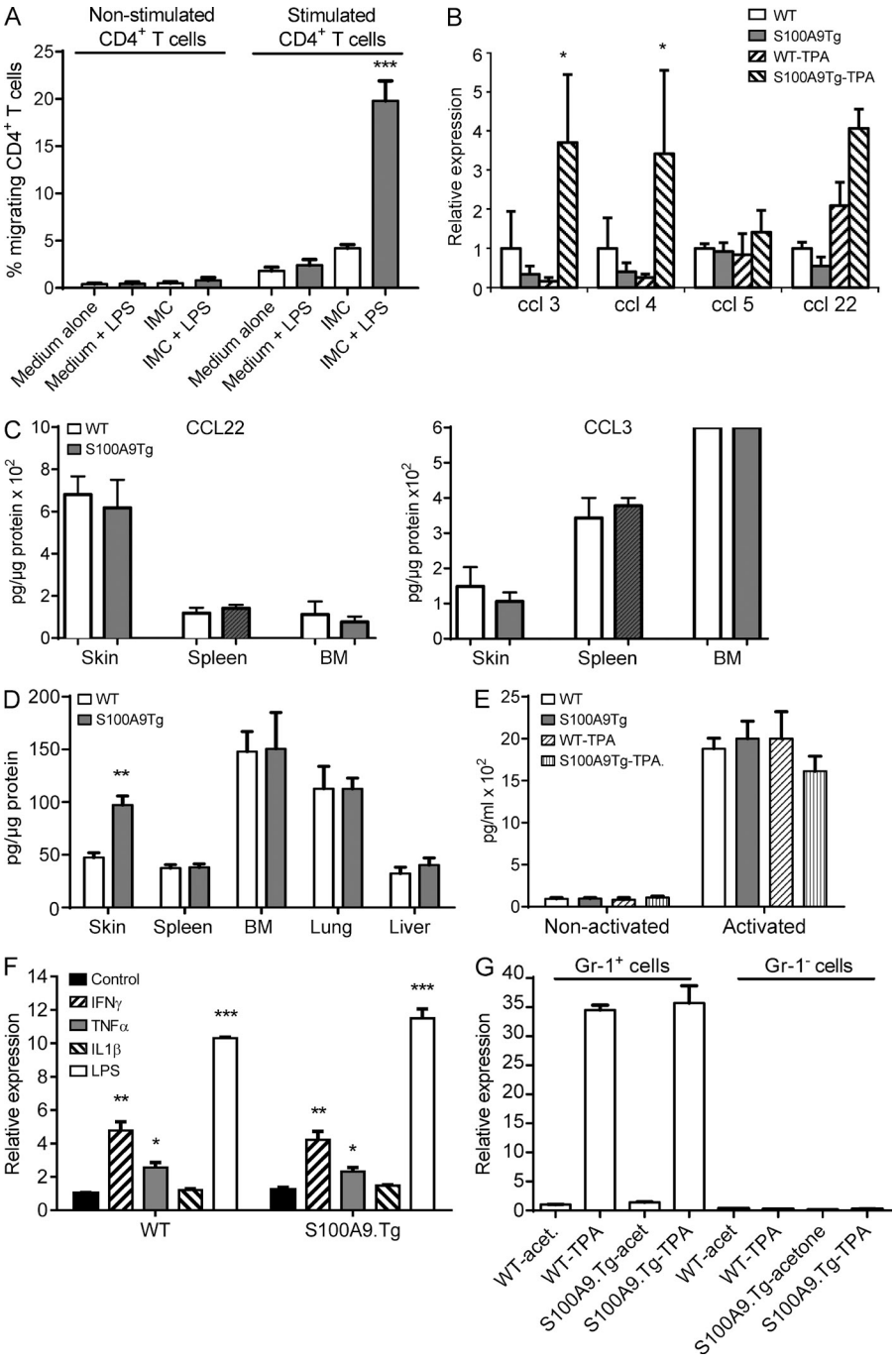

Figure 8. Skin IMCs release CD4+ T cell chemokine CCL4. (A) Chemotaxis of CD4+ T cells isolated from control mice to supernatant from IMCs. IMCs were either stimulated or not with LPS. T cells were stimulated or not with CD3/CD28 antibody. CD4+ T cells were placed in the top chamber and supernatants (30% vol/vol) in the bottom chamber. For control, LPS was added to the medium in the bottom chamber. Mean and SD of cumulative results of six independent experiments are shown. ***, $P < 0.001$. (B) Quantitative RT-PCR analysis of the expression of *ccl3*, *ccl4*, *ccl5*, and *ccl22* in skin of WT or S100A9Tg mice treated with TPA or acetone. Differences in expression of *ccl3* and *ccl4* were significant. Mean and SD are shown. *, $P < 0.01$. (C) Amount of CCL22 (left) and CCL3 (right) protein measured by ELISA in lysates of various organs from TPA-treated WT and S100A9Tg mice. Mean and SD from four experiments with three mice per group are shown. Each measurement was performed in duplicate and normalized for total protein. Cumulative results from three experiments are shown. (D) Amount of CCL4 protein measured by ELISA in lysates of various organs from TPA-treated WT and S100A9Tg mice. Mean and SD from four experiments with three mice per group are shown. Each measurement was performed in duplicate normalized for total protein. **, $P < 0.01$. (E) Amount of CCL4 determined by ELISA in supernatants of IMCs isolated from BM of WT or S100A9Tg mice treated with TPA for 4 wk. Cells were activated with LPS overnight. Measurements were performed twice in duplicates. Mean and SD are shown. (F) Expression of *ccl4* in Gr-1+CD11b+ IMCs isolated from BM of naive mice treated for 24 h with the indicated cytokines. The range of most commonly used concentrations was tested. Concentrations shown: 250 ng/ml IFN-γ, 50 ng/ml TNF, 50 ng/ml IL-1β, and 100 ng/ml LPS. *Ccl4* expression was measured by quantitative PCR and normalized to β-actin. Mean and SD are shown. *, $P < 0.05$; **, $P < 0.01$; ***, $P < 0.001$ from control ($n = 3$). (G) Expression of *ccl4* in Gr-1+ and Gr-1− cells isolated from skin of WT or S100A9Tg mice treated for 5 wk with TPA ($n = 3$). Mean and SD are shown.

(Fig. 8 B). However, no differences in the amount of CCL3 and CCL22 proteins were found in skin lysates of TPA-treated S100A9Tg and WT mice (Fig. 8 C). In contrast, the amount of CCL4 in the skin of TPA-treated S100A9Tg mice was significantly higher than in WT mice. No differences in the amount of CCL4 were observed in spleens, BM, lung, or liver (Fig. 8 D). Because skin was the primary site of IMC accumulation in TPA-treated S100A9Tg mice, these data are consistent with the role of IMCs as the primary source of CCL4. To verify that IMCs are indeed able to produce CCL4, this chemokine was measured in supernatants from BM IMCs isolated from TPA-treated WT and S100A9Tg mice. A large amount of CCL4 was found in supernatants from stimulated IMCs (Fig. 8 E). Next, we evaluated the nature of stimuli that could induce expression of *ccl4* in IMCs isolated from BM of naive mice. IMCs were treated for 24 h with several proinflammatory cytokines. IFN-γ caused more than fourfold up-regulation of *ccl4* expression. The effect of TNF was significant but less potent, whereas IL-1β at a selected concentration did not up-regulate *ccl4* expression in

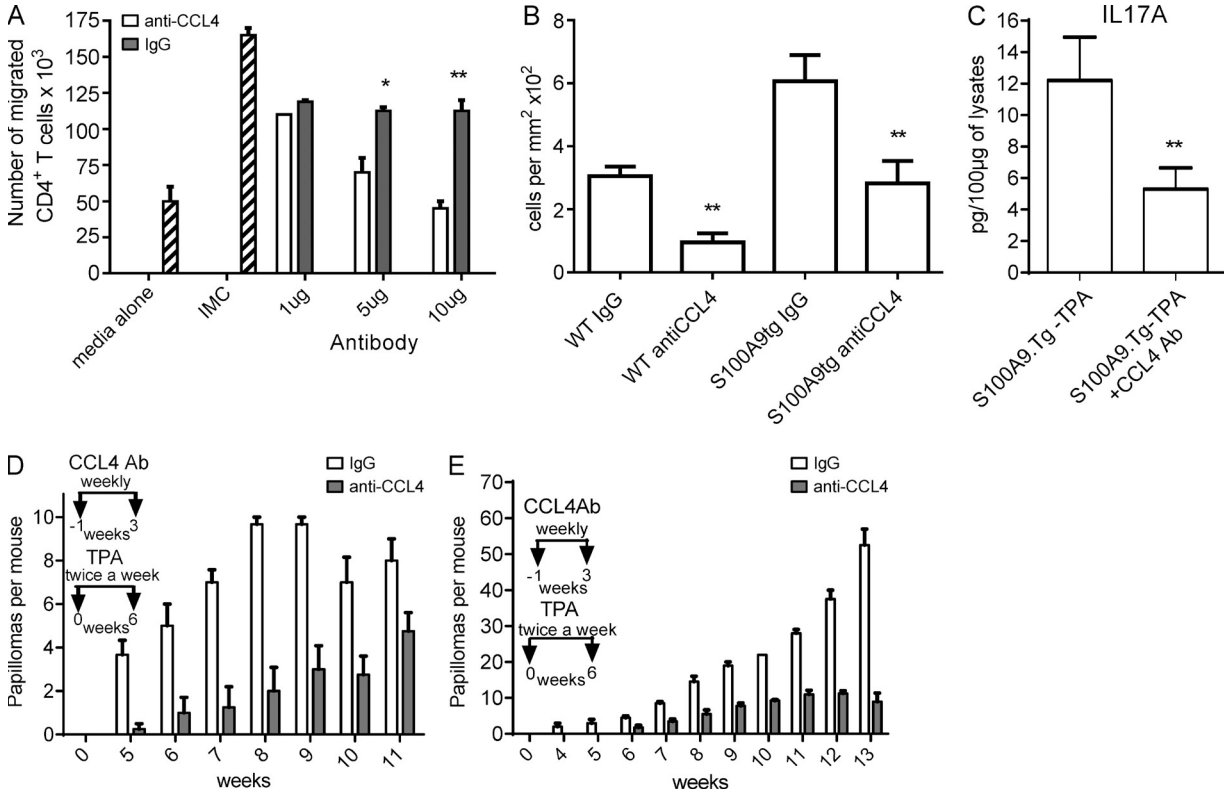

Figure 9. CCL4 is responsible for the recruitment of CD4+ T cells to the skin. (A) Neutralizing CCL4 antibody inhibited migration of activated CD4+ T cells toward supernatant obtained from LPS-stimulated IMCs. Concentrations of CCL4 antibody or IgG are shown in the graph. Two experiments were performed in duplicate. (B) S100A9Tg mice were treated for 4 wk with TPA and either control IgG or neutralizing CCL4 antibody. The number of CD4+ cells in the skin is shown. (C) The amount of IL-17A in the skin of S100A9Tg mice treated with CCL4 antibody. Each group included three mice. (A–C) Mean and SD are shown. *, $P < 0.05$; **, $P < 0.01$. (D and E) The number of papillomas formed in Tg.AC (D) and S100A9Tg;Tg.AC (E) mice treated with TPA and control IgG or CCL4 antibody as indicated. Mean and SD are shown. Each group included four mice. $P = 0.001$ (D) and $P < 0.001$ (E).

IMCs (Fig. 8 F). We assessed the expression of *ccl4* in cells isolated directly from skin of WT or S100A9Tg mice. Skin Gr-1+ IMCs from TPA-treated WT or S100A9Tg mice expressed a high level of *ccl4*, whereas no expression was detected in Gr-1− cells (Fig. 8 G).

To verify the role of CCL4 in CD4+ T cell recruitment by Gr-1+ myeloid cells, we added neutralizing CCL4 antibody to IMC supernatants in chemotaxis assay. CCL4-specific antibody abrogated CD4+ T cell migration caused by IMCs in a dose-dependent manner (Fig. 9 A). To test the role of CCL4 in vivo, WT and S100A9Tg mice were treated for 4 wk with control or CCL4 antibody concurrent with TPA. Treatment with CCL4 antibody did not affect the presence of Gr-1+ myeloid cells or CD8+ T cells in the skin (not depicted). In contrast, neutralization of CCL4 significantly ($P < 0.01$) reduced the presence of CD4+ T cells in WT and S100A9Tg skin (Fig. 9 B). CCL4 antibody significantly reduced the presence of IL-17A in the skin of S100A9Tg mice, strongly suggesting the link between CCL4-mediated CD4+ T cell migration and IL-17A presence in the skin (Fig. 9 C). Weekly treatment of Tg.AC mice with CCL4 antibody during the first 3 wk of TPA promotion significantly reduced the formation of tumors ($P < 0.01$; Fig. 9 D). Similar experiments were performed in S100A9Tg;Tg.AC bitransgenic mice who developed higher numbers of papillomas than Tg.AC mice, but the CCL4 antibody still drastically ($P < 0.01$) reduced the number of tumors (Fig. 9 E).

DISCUSSION

In this study, we report, for the first time, that granulocytic IMCs directly contribute to skin tumor development via recruitment of IL-17–producing CD4+ T cells (Th17 cells). Although the link between inflammation and cancer is well established (Arthur et al., 2012; Coussens et al., 2013), the contribution of specific cell populations to the initial phase of tumor development remains unclear. Previously, MΦs were shown to be involved in early stages of tumor development and progression (Hagemann and Balkwill, 2005; Sica and Bronte, 2007; Schmid and Varner, 2012). The role of MDSCs in tumor immune escape is now well established. In recent years, evidence pointed to expansion of MDSCs in chronic infection and inflammation (Cuenca et al., 2011; Nagaraj et al., 2013). This increase in MDSCs raised the question as to whether these cells could contribute to tumorigenesis. Our data demonstrated accumulation of a large number of CD33+S100A9+ cells (the phenotype typical for MDSCs) in

tissues of patients with inflammatory conditions, which predisposes to the development of cancers. Accumulation of these cells was more prominent than that of mature neutrophils and MΦs.

Because inflammation is a complex process, the specific role of individual cell populations in tumor promotion is difficult to ascertain. S100A9Tg mice provide a novel experimental model in which tissue accumulation of cells with the IMC phenotype is not caused by infection, trauma, or cancer. The vast majority of myeloid cells accumulated in skin of S100A9Tg were granulocytic IMCs, which is consistent with the concept that overexpression of S100A9 in myeloid precursors inhibits differentiation of myeloid precursors to DCs, and to some extent MΦs, and promotes appearance of immature granulocytes. Activated keratinocytes can attract granulocytes via release of CXCL8 chemokine (Huang et al., 2011). This chemokine may provide a signal for initial influx of IMCs to TPA-treated skin. Our results with BM transfers and Gr-1–specific antibody depletions in S100A9Tg mice, as well as decreased skin carcinogenesis in S100A9KO mice, demonstrate that IMCs were the primary facilitator of tumor development in this experimental system. Our data in S100A9KO mice are not consistent with a recent study indicating that S100A9 had a protective role in inflammation-induced skin carcinogenesis (McNeill and Hogg, 2014). Whether differences were caused by differences in the mouse models or other factors needs to be elucidated. IMCs accumulated in skin of mice lack immune-suppressive activity and thus cannot be defined as MDSCs. These results were consistent with recent findings of accumulation of myeloid cells with a phenotype similar to that of MDSCs but lacking immune-suppressive activity in mice exposed to cigarette smoke (Ortiz et al., 2014). These cells acquired immune-suppressive activity only after the development of lung tumors (Ortiz et al., 2014). Our data demonstrated that although the number of DCs migrating from skin to LN in S100A9Tg mice was decreased, the priming of $CD8^+$ T cells to antigen applied over the skin was not affected. Apparently, the modest decrease in DCs in skin was not sufficient to inhibit $CD8^+$ T cell priming. Alternatively, the significantly higher proportion of $CD11b^-CD207^+CD103^+$ DCs in S100A9Tg mice may have compensated for decrease of other DC subsets because these cells play a major role in cross-presentation of antigens in the skin (Henri et al., 2010). Collectively, these data indicate that enhanced papilloma formation in S100A9Tg mice is not caused by myeloid cell–mediated immune suppression as typically observed with MDSCs in cancer.

Granulocytic cells may contribute to neoplastic transformation by increasing the rate of mutation and proliferation of epithelial cells via release of reactive oxygen species (Marnett, 2000; Le'Negrate et al., 2003; Balkwill, 2009), activation of cyclooxygenase-2 (Kim et al., 2005), and inhibition of nucleotide excision repair by myeloperoxidase (Gasche et al., 2001; Hofseth et al., 2003; Güngör et al., 2007). In this study, we did not evaluate the malignant conversion of tumor lesions but focused on the earlier premalignant events promoting papilloma formation. We found that granulocytic IMCs recruited $CD4^+$ T cells to the site of their accumulation. Importantly, only activated IMCs were able to recruit $CD4^+$ T cells. Our data indicated that IMCs did not specifically recruit Th17 $CD4^+$ T cells or cause their conversion from precursors, but rather recruited these cells as part of large pool of $CD4^+$ T cells. It was associated with dramatic decrease in IL-13–producing $CD4^+$ T cells. IL-13 was previously shown to be a negative regulator of Th17 cells (Newcomb et al., 2009). This resulted in significant increase of IL-17 but not IL-22 in the skin of S100A9Tg mice as compared with WT mice. Depletion of $CD4^+$ T cells or IL-17 in S100A9Tg mice abrogated induction of papilloma formation. These data strongly indicate that $CD4^+$ T cells and IL-17 mediated the effect of IMCs on tumor development.

The role of $CD4^+$ T cells in tumor progression remains enigmatic and thus requires further investigation. The $CD4^+$ T cell deficiency on one hand enhanced cancer progression in methylcholanthrene (MCA)-initiated sarcoma development (Koebel et al., 2007; DeNardo et al., 2010), whereas on the other hand, it inhibited tumor development in the two-stage squamous carcinogenesis model (Girardi et al., 2003). Similarly, in the K14HPV16 skin cancer model, with E6/E7 oncogenes expressed in epidermis from keratin 14 promoter, $CD4^+$ T cell deficiency modestly attenuated neoplastic progression, whereas cervical carcinoma development was significantly enhanced (Daniel et al., 2003, 2005). However, there are studies suggesting that IL-17 and IL-22 produced by Th17 cells contribute to tumor development by inducing angiogenesis or directly affecting keratinocyte proliferation and survival (Heidenreich et al., 2009; Cho et al., 2012; Fujita, 2013). IL-17 also promotes accumulation of cells with MDSC phenotype (He et al., 2010), suggesting a feedback mechanism. IL-17 KO mice in a two-stage carcinogenesis model showed delayed papilloma formation compared with WT mice (Xiao et al., 2009; Wang et al., 2010).

We identified CCL4 chemokine as the main factor responsible for IMC-mediated recruitment of $CD4^+$ T cells. CCL4 or MIP-1β is a 69-aa member of the β (CC) family of chemokines. It is produced by various cells, including myeloid cells, and binds to CCR1, CCR5, and US28 receptors. Melanoma-associated MDSCs produce high levels of CCL4 among other chemokines, and in CCR5-deficient mice growth of transplantable tumors was delayed (Schlecker et al., 2012). Activated $CD4^+$ T cells up-regulate CCR5 receptor, allowing these cells to be recruited to the site of CCL4 production (Castellino et al., 2006), which is consistent with our finding that IMCs attracted only activated $CD4^+$ T cells. Although it was reported that different $CD4^+$ T cell subsets may express unique repertoires of chemokine receptors, current evidence suggests that CCR5 can be expressed on recently activated cells of any subset (Bromley et al., 2008), consistent with lack of preferential accumulation of specific populations of $CD4^+$ T cells in the skin of S100A9Tg mice.

Our data suggest a sequence of events that promote tumor formation in skin and possibly other tissues. Granulocytic

IMCs accumulate at the site of cutaneous irritation or inflammation. Activated IMCs release CCL4 that recruits $CD4^+$ T cells, including proinflammatory populations. These T cells release IL-17 to stimulate proliferation of keratinocytes, which contribute to tumor formation. The direct effect of IMCs on keratinocytes or epithelial cells in other tissues merits further investigation, as well as the possibility that targeting IMCs may benefit individuals with high risk of cancer development.

MATERIALS AND METHODS

Patient samples. De-identified colon tissues slides were obtained from St. Mark's Hospital (Harrow, England, UK). Samples were taken from patients after obtaining informed consent and with the approval of the Outer West London Research Ethics Committee (UK). It included six samples obtained from normal colonic biopsies (control), five samples from patients with ulcerative colitis showing low- and high-grade dysplasia, and six samples from patients with colorectal cancer (moderately differentiated adenocarcinoma). Paraffin-embedded tissue blocks were retrieved using an approved Institutional Review Board protocol for de-identified archived skin biopsies through the Department of Dermatology, National Institutes of Health Skin Disease Research Center Tissue Acquisition Core (P30-AR057217), Perelman School of Medicine, University of Pennsylvania (Philadelphia, PA). It included five samples from normal skin (control), five samples from patients with lichen planus, five patients with psoriasis, five patients with spongiotic dermatitis (eczema), five patients with BCC, and five patients with melanoma.

After deparaffinization, rehydration, and blocking endogenous peroxides with fixation with 5% hydrogen peroxide in methanol, heat-induced antigen retrieval was performed using Tris-EDTA buffer. For evaluation of $S100A9^+CD33^+$ cells, tissues were stained with S100A9 antibody (diluted 1:500 in 5% BSA; Novus Biologicals) and CD33 antibody (dilution 1:100 in 5% BSA; Novocastra) followed by Alexa Fluor 594 antibody (dilution 1:400 in 5% BSA; Life Technologies) and Alexa Fluor 647 antibody (dilution 1:400 in 5% BSA; Life Technologies). For neutrophils and MΦs, a single staining protocol was used. Neutrophils were stained with neutrophil elastase antibody (dilution 1:2,000 in 5% BSA; Abcam) and MΦs with CD163 antibody (dilution 1:200 in 5% BSA; Abcam). Alexa Fluor 594 (Life Technologies) anti–rabbit antibody was used as secondary. Cell nuclei were stained with DAPI (dilution 1:5,000 in PBS; Life Technologies). Cells were analyzed using a TCS SP5 confocal microscope (Leica) and E600 upright microscope (Nikon). The number of cells per square millimeter of tissue was calculated in at least five fields using Image pro plus software (Media Cybernetics). Positive stained cells were normalized to total nuclear cell count using DAPI.

Mice. All animal experiments were approved by the University of South Florida Institutional Animal Care and Use Committee. Mice were housed in pathogen-free facilities. Tg.AC mice described previously (Tepper et al., 1990) were obtained from Taconic. S100A9Tg mice on FVB/N background (Cheng et al., 2008) and S100A9KO mice on C57BL/6 background (Manitz et al., 2003) were described previously. BALB/c, C57BL/6, and FVB/N mice were obtained from the National Cancer Institute, and OT-1 mice were obtained from the Jackson Laboratory. In S100A9Tg;Tg.AC bitransgenic mice, the presence of S100A9-IRES-GFP transgene was verified by the expression of GFP in leukocytes from peripheral blood, and the *v-h-ras* transgene was detected by genomic PCR for the SV40 sequences. In some experiments, S100A9Tg mice on C57BL/6 background were used after backcrossing S100A9Tg FVB/N mice with C57BL/6 mice for nine generations.

Skin carcinogenesis. Female, aged-matched (7–10 wk old) littermate mice were used in experiments with Tg.AC and S100A9Tg;Tg.AC mice. Dorsal skin was shaved, and 3 nmol TPA (Sigma-Aldrich) in 200 µl acetone vehicle was applied twice a week for 4 or 6 wk. In the carcinogenesis model in C57BL/6 WT or S100A9KO mice, 100-nmol single dose of DMBA was topically applied, followed by 10 nmol TPA every 24 h for 12 wk, as previously described (Gebhardt et al., 2008). Papillomas were assessed weekly and counted when they reached 1 mm for at least 2 wk. In BM transfer experiments, lethally irradiated (950 rads) mice were injected i.v. with 10^6 BM cells from donor mice. Treatment with TPA or DMBA plus TPA as described above was started 3 wk after the BM transfer.

Tissue preparation and histology. Skin pieces were snap-frozen, and slides were fixed with acetone and blocked overnight with 10% goat serum, 1% BSA, and 2.5% mouse serum in PBS at room temperature. The primary antibodies from BD were used at 1:100 dilutions: Gr1 (RB6-8C5), CD4 (H129.19), and CD8 (53-6.7). The antibodies from eBioscience were used at 1:50 dilution: CD11c (N418) and F4/80 (BM8). Biotinylated anti–rat IgG (Vector Laboratories) or anti–hamster IgG (Vector Laboratories) was used as a secondary antibody. Alkaline phosphatase kit and Vector Red substrate (Vector Laboratories) were used for visualization of the results. The tissues were counterstained with hematoxylin. Images were taken by the digital slide scanner Scanscope (Aperio) and analyzed by Aperio software. Cell number was calculated per 1 mm^2. The antibodies specific for γδ T cells (GL-3), cytokeratin-14 (LL002), and Ki67 (SP6) were purchased from Abcam, and the staining was evaluated on an E600 upright microscope.

Cytokine expression. For the analysis of gene expression, total RNA was extracted with TRIzol reagent (Invitrogen), and cDNA was synthesized using the High Capacity cDNA Reverse transcription kit (Applied Biosystems). To detect chemokines, PCR was performed with 2 µl cDNA and 12.5 µl SYBR Master Mixture (Applied Biosystems) using specific primers: *Cd2*, 5′-CCCAATGAGTAGGCTGGAGA-3′ and 5′-AAAATGGATCCAC-ACCTTGC-3′; *Ccl3*, 5′-CCAAGTCTTCTCAGCGCCATA-3′ and 5′-GATGAATTGGCGTGGAATCTTC-3′; *Ccl4*, 5′-TGCTCGTGG-CTGCCTTCT-3′ and 5′-CTGCCGGGAGGTGTAAGAGA-3′; *Ccl5*, 5′-TGCCCACGTCAAGGAGTATT-3′ and 5′-CAGGACCGGAGT-GGGAGTA-3′; *Ccl9*, 5′-GATGAAGCCCTTTCATACTGC-3′ and 5′-GTGGTTGTGAGTTTTGCTCCAATC-3′; and *Ccl22*, 5′-GTGGC-TCTCGTCCTTCTTGC-3′ and 5′-GGACAGTTTATGGAGTAGCTT-3′. Amplification of endogenous β-actin was used as an internal control.

For evaluation of the proteins, tissues were homogenized in RIPA buffer, and BM cells were flushed out for protein extraction. Chemokines were measured by ELISA using the kits from PeproTech: CCL3, CCL4, or CCL22. CCL4 was also measured using an R&D Systems kit. Likewise, the cytokines (IL10, IL17A, and IL22) in skin, spleen, and BM were measured by ELISA using the kits from eBioscience.

Western blot. Samples (30 µg protein per lane) were subjected to electrophoresis in 12% SDS-polyacrylamide gels and then blotted onto PVDF membranes. Membranes were blocked for 1 h at room temperature with 5% dry skim milk in TBS (20 mM Tris-HCl, pH 7.6, and 137 mM NaCl plus 0.1% [vol/vol] Tween 20) and then probed with S100A9 or β-actin–specific antibodies (Santa Cruz Biotechnology, Inc.), followed by secondary antibody conjugated with horseradish peroxidase. Results were visualized by chemiluminescence detection (GE Healthcare).

Depletion of cells and neutralization of chemokines in vivo. Mice were injected i.p. with 250 µg CD4 (clone: GK1.5; Bio X Cell) and Gr-1 (clone: RB6-8C5; Bio X Cell). Injections were performed once a week for 4 wk starting 1 wk before the beginning of TPA treatment. For neutralization of CCL4 and IL17A, 100 µg CCL4 (R&D Systems)- or 200 µg IL-17A (clone: 17F3; Bio X Cell)–specific monoclonal antibodies were used. Control groups in CD4 and Gr-1 depletion and neutralization experiments received rat IgG2b isotype (clone: LTF2; Bio X Cell); controls for IL17A neutralization experiments received mouse IgG (Sigma-Aldrich), whereas controls in CCL4 neutralization experiments received goat IgG (R&D Systems).

$CD4^+$ T cell polarization experiments. Naive $CD62L^+CD4^+$ T cells were isolated from spleen of FVB/N mice using magnetic beads (Miltenyi Biotec) and co-culture with $Gr\text{-}1^+$ cells isolated from BM of WT or S100A9Tg

mice treated for 4 wk with TPA. Cells were activated for 4 d at 37°C with CD3/CD28 beads. On day 4, cells were stimulated with 50 ng/ml TPA and 700 ng/ml ionomycin for 4 h in the presence of protein transport inhibitor GolgiStop (BD) to prevent cytokine secretion during the last 3 h. The cells were harvested, followed by intracellular staining with CD4, IL-17, IL-4, FoxP3, or IFN-γ antibodies (all from BD) and analysis by flow cytometry.

Skin cell isolation and analysis. Pieces of shaved skin were incubated in PBS containing 0.2% trypsin for 30 min at 37°C, cut into small pieces, and incubated with 0.8 mg/ml collagenase in RPMI for 40 min at 37°C. Single cell suspension was prepared by pressing tissues through a 100-µm cell strainer. For analysis of the cell phenotype, cells were used directly for flow cytometry. Nonspecific staining was blocked by Fc-block (BD), and staining was performed in 1% FBS. The cells were analyzed by flow cytometry using an LSRII cytometer (BD) and FlowJo software (8.6). Dead cells were excluded by DAPI staining, and $CD45^+$ cells were analyzed. For the analysis of intracellular cytokines, mononuclear cells were isolated by density centrifugation on Ficoll-Paque, washed, and plated at 2×10^6/ml concentration in round-bottom 96-well plates. Cells were then stimulated with 30 ng/ml TPA and 750 ng/ml ionomycin for 4 h, the last 3 h in the presence of GolgiStop. Cells were stained by Live-Dead Violet (Life Technologies), followed by CD45 and CD4 antibodies. After fixation and permeation, cells were stained for intracellular cytokines or FoxP3 and analyzed by flow cytometry. For the isolation of myeloid cells from skin, the shaved skin was cut and washed with PBS buffer. The subcutaneous fat was scrapped off using a scalpel, and the skin tissue was divided into three to four pieces. The epidermis and dermal layer were enzymatically digested and subsequently dissociated into single cell suspension using a gentleMACS dissociator (Miltenyi Biotec). IMCs were purified from single cell suspension using biotinylated anti–Gr-1 antibody (Miltenyi Biotec), followed by streptavidin microbeads. $Ly6G^+$ granulocytic IMCs were isolated from the skin using the Epidermis Dissociation kit (Miltenyi Biotec).

Chemotaxis. $Gr\text{-}1^+$ cells were isolated from BM using biotinylated anti–Gr-1 antibody and streptavidin microbeads (Miltenyi Biotec). The purity of $Gr\text{-}1^+CD11b^+$ cells was >95%. Cells were cultured overnight in serum-free medium (Cellgenix) at 10^6/ml, in the presence or absence of 0.5 µg/ml LPS. Supernatants were collected after 24 h and added at 30% vol/vol to the bottom chamber of Transwell plates (5-µm pores) in a total volume of 500 µl serum-free medium. To activate T cells, splenocytes were cultured with 0.5 µg/ml anti-CD3 antibody for 3 d in serum-free medium. One million stimulated or nonstimulated splenocytes were resuspended in 100 µl serum-free medium and added to the top chamber of the Transwell. After 4-h incubation at 37°C, $CD4^+$ T cells that passed through the membrane to the lower chamber were measured by flow cytometry.

LC staining. Epidermal sheets were prepared from dorsal skin as previously described (Gabrilovich et al., 1994). The epidermal sheets were fixed in acetone for 1 min, blocked with 1% BSA and Fc-block, and stained overnight at 4°C with IA/IE-PE antibody (clone 2G9; BD) at 1:100 dilution. The next day, sheets were washed, stained with secondary antibody, and mounted on slides. The staining was analyzed in an SP5 confocal microscope.

DC migration and T cell proliferation. Shaved dorsal skin was painted with 0.4 ml of a 1:1 mixture of acetone/DBP containing 250 µM DDAO (Invitrogen). 24 h later, draining LNs were collected and treated with 1 mg/ml collagenase in PBS/BSA for 30 min, and single cell suspensions were stained and analyzed by flow cytometry.

For the analysis of in vitro cell proliferation, 10^5 splenocytes from BALB/c mice (responders) were mixed with 10^5 T cell–depleted and irradiated (20Gy) splenocytes from FVB/N mice (stimulators) in U-bottom 96-well plates. $Gr\text{-}1^+$ cells from TPA-treated S100A9Tg or WT mice were added into wells at different ratios. On day 4, cells were pulsed with [^{3}H]thymidine (1 µCi/well; GE Healthcare) for 18 h. [^{3}H]thymidine uptake was counted using a liquid scintillation counter and expressed as counts per minute.

For the assessment of in vivo T cell proliferation in response to antigens, splenocytes and LN cells collected from OT-1 $CD45.1^+$ mice were labeled with 5 µM DDAO. Eight million DDAO-labeled OT-1 cells were injected into the tail vein of C57BL/6 ($CD45.2^+$) WT and S100A9Tg mice that were pretreated for 4 wk with TPA. The day after transfer, 10 mg OVA protein in 500 µl Ultrasicc gel was applied onto the shaved dorsal skin of the mice. 3 d later, skin-draining LNs and spleen were collected. Cells were stained and analyzed by flow cytometry.

Statistical analysis. Statistical analysis was performed using an unpaired two-tailed Student's *t* test with significance determined at $P < 0.05$. For the analysis of papilloma formation, statistical significance of repeated measurements was assessed using a two-way ANOVA test.

Support was provided by Wistar Institute imaging and flow cytometry cores.

This paper was supported by National Institutes of Health (NIH) grant CA 100062 to D. Gabrilovich and, in part, by P50 CA168536. E. Celis was supported by NIH grant R01CA157303.

The authors declare no competing financial interests.

Submitted: 1 May 2014
Accepted: 22 January 2015

REFERENCES

Arthur, J.C., E. Perez-Chanona, M. Mühlbauer, S. Tomkovich, J.M. Uronis, T.J. Fan, B.J. Campbell, T. Abujamel, B. Dogan, A.B. Rogers, et al. 2012. Intestinal inflammation targets cancer-inducing activity of the microbiota. *Science*. 338:120–123. http://dx.doi.org/10.1126/science.1224820

Balkwill, F. 2009. Tumour necrosis factor and cancer. *Nat. Rev. Cancer.* 9:361–371. http://dx.doi.org/10.1038/nrc2628

Bierie, B., and H.L. Moses. 2010. Transforming growth factor beta (TGF-β) and inflammation in cancer. *Cytokine Growth Factor Rev.* 21:49–59. http://dx.doi.org/10.1016/j.cytogfr.2009.11.008

Brandau, S., S. Trellakis, K. Bruderek, D. Schmaltz, G. Steller, M. Elian, H. Suttmann, M. Schenck, J. Welling, P. Zabel, and S. Lang. 2011. Myeloid-derived suppressor cells in the peripheral blood of cancer patients contain a subset of immature neutrophils with impaired migratory properties. *J. Leukoc. Biol.* 89:311–317. http://dx.doi.org/10.1189/jlb.0310162

Bromley, S.K., T.R. Mempel, and A.D. Luster. 2008. Orchestrating the orchestrators: chemokines in control of T cell traffic. *Nat. Immunol.* 9:970–980. http://dx.doi.org/10.1038/ni.f.213

Castellino, F., A.Y. Huang, G. Altan-Bonnet, S. Stoll, C. Scheinecker, and R.N. Germain. 2006. Chemokines enhance immunity by guiding naive $CD8^+$ T cells to sites of $CD4^+$ T cell–dendritic cell interaction. *Nature.* 440:890–895. http://dx.doi.org/10.1038/nature04651

Chen, X., E.A. Eksioglu, J. Zhou, L. Zhang, J. Djeu, N. Fortenbery, P. Epling-Burnette, S. Van Bijnen, H. Dolstra, J. Cannon, et al. 2013. Induction of myelodysplasia by myeloid-derived suppressor cells. *J. Clin. Invest.* 123:4595–4611. http://dx.doi.org/10.1172/JCI67580

Cheng, P., C.A. Corzo, N. Luetteke, B. Yu, S. Nagaraj, M.M. Bui, M. Ortiz, W. Nacken, C. Sorg, T. Vogl, et al. 2008. Inhibition of dendritic cell differentiation and accumulation of myeloid-derived suppressor cells in cancer is regulated by S100A9 protein. *J. Exp. Med.* 205:2235–2249. http://dx.doi.org/10.1084/jem.20080132

Cho, K.A., J.Y. Kim, S.Y. Woo, H.J. Park, K.H. Lee, and C.U. Pae. 2012. Interleukin-17 and interleukin-22 induced proinflammatory cytokine production in keratinocytes via inhibitor of nuclear factor κB kinase-α expression. *Ann. Dermatol.* 24:398–405. http://dx.doi.org/10.5021/ad.2012.24.4.398

Coussens, L.M., L. Zitvogel, and A.K. Palucka. 2013. Neutralizing tumor-promoting chronic inflammation: a magic bullet? *Science.* 339:286–291. http://dx.doi.org/10.1126/science.1232227

Cuenca, A.G., M.J. Delano, K.M. Kelly-Scumpia, C. Moreno, P.O. Scumpia, D.M. Laface, P.G. Heyworth, P.A. Efron, and L.L. Moldawer. 2011. A paradoxical role for myeloid-derived suppressor cells in sepsis and trauma. *Mol. Med.* 17:281–292. http://dx.doi.org/10.2119/molmed.2010.00178

Dalgleish, A.G., and K. O'Byrne. 2006. Inflammation and cancer: the role of the immune response and angiogenesis. *Cancer Treat. Res.* 130:1–38. http://dx.doi.org/10.1007/0-387-26283-0_1

Daniel, D., N. Meyer-Morse, E.K. Bergsland, K. Dehne, L.M. Coussens, and D. Hanahan. 2003. Immune enhancement of skin carcinogenesis by $CD4^+$ T cells. *J. Exp. Med.* 197:1017–1028. http://dx.doi.org/10.1084/jem.20021047

Daniel, D., C. Chiu, E. Giraudo, M. Inoue, L.A. Mizzen, N.R. Chu, and D. Hanahan. 2005. $CD4^+$ T cell-mediated antigen-specific immunotherapy in a mouse model of cervical cancer. *Cancer Res.* 65:2018–2025. http://dx.doi.org/10.1158/0008-5472.CAN-04-3444

DeNardo, D.G., P. Andreu, and L.M. Coussens. 2010. Interactions between lymphocytes and myeloid cells regulate pro- versus anti-tumor immunity. *Cancer Metastasis Rev.* 29:309–316. http://dx.doi.org/10.1007/s10555-010-9223-6

Dyer, R.K., M.A. Weinstock, T.S. Cohen, A.E. Rizzo, and S.F. Bingham; VATTC Trial Group. 2012. Predictors of basal cell carcinoma in high-risk patients in the VATTC (VA Topical Tretinoin Chemoprevention) trial. *J. Invest. Dermatol.* 132:2544–2551. http://dx.doi.org/10.1038/jid.2012.227

Dyson, J.K., and M.D. Rutter. 2012. Colorectal cancer in inflammatory bowel disease: what is the real magnitude of the risk? *World J. Gastroenterol.* 18:3839–3848. http://dx.doi.org/10.3748/wjg.v18.i29.3839

Ehrchen, J.M., C. Sunderkötter, D. Foell, T. Vogl, and J. Roth. 2009. The endogenous Toll-like receptor 4 agonist S100A8/S100A9 (calprotectin) as innate amplifier of infection, autoimmunity, and cancer. *J. Leukoc. Biol.* 86:557–566. http://dx.doi.org/10.1189/jlb.1008647

Feng, P.H., K.Y. Lee, Y.L. Chang, Y.F. Chan, L.W. Kuo, T.Y. Lin, F.T. Chung, C.S. Kuo, C.T. Yu, S.M. Lin, et al. 2012. $CD14^+S100A9^+$ monocytic myeloid-derived suppressor cells and their clinical relevance in non-small cell lung cancer. *Am. J. Respir. Crit. Care Med.* 186:1025–1036. http://dx.doi.org/10.1164/rccm.201204-0636OC

Fridlender, Z.G., J. Sun, S. Kim, V. Kapoor, G. Cheng, L. Ling, G.S. Worthen, and S.M. Albelda. 2009. Polarization of tumor-associated neutrophil phenotype by TGF-β: "N1" versus "N2" TAN. *Cancer Cell.* 16:183–194. http://dx.doi.org/10.1016/j.ccr.2009.06.017

Fujita, H. 2013. The role of IL-22 and Th22 cells in human skin diseases. *J. Dermatol. Sci.* 72:3–8. http://dx.doi.org/10.1016/j.jdermsci.2013.04.028

Gabrilovich, D.I., and S. Nagaraj. 2009. Myeloid-derived suppressor cells as regulators of the immune system. *Nat. Rev. Immunol.* 9:162–174. http://dx.doi.org/10.1038/nri2506

Gabrilovich, D.I., G.M. Woods, S. Patterson, J.J. Harvey, and S.C. Knight. 1994. Retrovirus-induced immunosuppression via blocking of dendritic cell migration and down-regulation of adhesion molecules. *Immunology.* 82:82–87.

Gabrilovich, D.I., S. Ostrand-Rosenberg, and V. Bronte. 2012. Coordinated regulation of myeloid cells by tumours. *Nat. Rev. Immunol.* 12:253–268. http://dx.doi.org/10.1038/nri3175

Gasche, C., C.L. Chang, J. Rhees, A. Goel, and C.R. Boland. 2001. Oxidative stress increases frameshift mutations in human colorectal cancer cells. *Cancer Res.* 61:7444–7448.

Gebhardt, C., A. Riehl, M. Durchdewald, J. Németh, G. Fürstenberger, K. Müller-Decker, A. Enk, B. Arnold, A. Bierhaus, P.P. Nawroth, et al. 2008. RAGE signaling sustains inflammation and promotes tumor development. *J. Exp. Med.* 205:275–285. http://dx.doi.org/10.1084/jem.20070679

Girardi, M., E. Glusac, R.B. Filler, S.J. Roberts, I. Propperova, J. Lewis, R.E. Tigelaar, and A.C. Hayday. 2003. The distinct contributions of murine T cell receptor (TCR)$\gamma\delta^+$ and TCR$\alpha\beta^+$ T cells to different stages of chemically induced skin cancer. *J. Exp. Med.* 198:747–755. http://dx.doi.org/10.1084/jem.20021282

Güngör, N., R.W. Godschalk, D.M. Pachen, F.J. Van Schooten, and A.M. Knaapen. 2007. Activated neutrophils inhibit nucleotide excision repair in human pulmonary epithelial cells: role of myeloperoxidase. *FASEB J.* 21:2359–2367. http://dx.doi.org/10.1096/fj.07-8163com

Hagemann, T., and F. Balkwill. 2005. MIFed about cancer? *Gastroenterology.* 129:1785–1787. http://dx.doi.org/10.1053/j.gastro.2005.09.039

He, D., H. Li, N. Yusuf, C.A. Elmets, J. Li, J.D. Mountz, and H. Xu. 2010. IL-17 promotes tumor development through the induction of tumor promoting microenvironments at tumor sites and myeloid-derived suppressor cells. *J. Immunol.* 184:2281–2288. http://dx.doi.org/10.4049/jimmunol.0902574

Heidenreich, R., M. Röcken, and K. Ghoreschi. 2009. Angiogenesis drives psoriasis pathogenesis. *Int. J. Exp. Pathol.* 90:232–248. http://dx.doi.org/10.1111/j.1365-2613.2009.00669.x

Henri, S., L.F. Poulin, S. Tamoutounour, L. Ardouin, M. Guilliams, B. de Bovis, E. Devilard, C. Viret, H. Azukizawa, A. Kissenpfennig, and B. Malissen. 2010. $CD207^+$ $CD103^+$ dermal dendritic cells cross-present keratinocyte-derived antigens irrespective of the presence of Langerhans cells. *J. Exp. Med.* 207:189–206. http://dx.doi.org/10.1084/jem.20091964

Hofseth, L.J., S. Saito, S.P. Hussain, M.G. Espey, K.M. Miranda, Y. Araki, C. Jhappan, Y. Higashimoto, P. He, S.P. Linke, et al. 2003. Nitric oxide-induced cellular stress and p53 activation in chronic inflammation. *Proc. Natl. Acad. Sci. USA.* 100:143–148. http://dx.doi.org/10.1073/pnas.0237083100

Huang, Y., L. Lin, A. Shanker, A. Malhotra, L. Yang, M.M. Dikov, and D.P. Carbone. 2011. Resuscitating cancer immunosurveillance: selective stimulation of DLL1-Notch signaling in T cells rescues T-cell function and inhibits tumor growth. *Cancer Res.* 71:6122–6131. http://dx.doi.org/10.1158/0008-5472.CAN-10-4366

Humble, M.C., C.S. Trempus, J.W. Spalding, R.E. Cannon, and R.W. Tennant. 2005. Biological, cellular, and molecular characteristics of an inducible transgenic skin tumor model: a review. *Oncogene.* 24:8217–8228. http://dx.doi.org/10.1038/sj.onc.1209000

Ichikawa, M., R. Williams, L. Wang, T. Vogl, and G. Srikrishna. 2011. S100A8/A9 activate key genes and pathways in colon tumor progression. *Mol. Cancer Res.* 9:133–148. http://dx.doi.org/10.1158/1541-7786.MCR-10-0394

Källberg, E., M. Stenström, D. Liberg, F. Ivars, and T. Leanderson. 2012. $CD11b^+Ly6C^{++}Ly6G^-$ cells show distinct function in mice with chronic inflammation or tumor burden. *BMC Immunol.* 13:69. http://dx.doi.org/10.1186/1471-2172-13-69

Kim, S.F., D.A. Huri, and S.H. Snyder. 2005. Inducible nitric oxide synthase binds, S-nitrosylates, and activates cyclooxygenase-2. *Science.* 310:1966–1970. http://dx.doi.org/10.1126/science.1119407

Koebel, C.M., W. Vermi, J.B. Swann, N. Zerafa, S.J. Rodig, L.J. Old, M.J. Smyth, and R.D. Schreiber. 2007. Adaptive immunity maintains occult cancer in an equilibrium state. *Nature.* 450:903–907. http://dx.doi.org/10.1038/nature06309

Le'Negrate, G., P. Rostagno, P. Auberger, B. Rossi, and P. Hofman. 2003. Downregulation of caspases and Fas ligand expression, and increased lifespan of neutrophils after transmigration across intestinal epithelium. *Cell Death Differ.* 10:153–162. http://dx.doi.org/10.1038/sj.cdd.4401110

Leder, A., A. Kuo, R.D. Cardiff, E. Sinn, and P. Leder. 1990. v-Ha-ras transgene abrogates the initiation step in mouse skin tumorigenesis: effects of phorbol esters and retinoic acid. *Proc. Natl. Acad. Sci. USA.* 87:9178–9182. http://dx.doi.org/10.1073/pnas.87.23.9178

Manitz, M.P., B. Horst, S. Seeliger, A. Strey, B.V. Skryabin, M. Gunzer, W. Frings, F. Schönlau, J. Roth, C. Sorg, and W. Nacken. 2003. Loss of S100A9 (MRP14) results in reduced interleukin-8-induced CD11b surface expression, a polarized microfilament system, and diminished responsiveness to chemoattractants in vitro. *Mol. Cell. Biol.* 23:1034–1043. http://dx.doi.org/10.1128/MCB.23.3.1034-1043.2003

Markowitz, J., and W.E. Carson III. 2013. Review of S100A9 biology and its role in cancer. *Biochim. Biophys. Acta.* 1835:100–109. http://dx.doi.org/10.1016/j.bbcan.2012.10.003

Marnett, L.J. 2000. Oxyradicals and DNA damage. *Carcinogenesis.* 21:361–370. http://dx.doi.org/10.1093/carcin/21.3.361

McNeill, E., and N. Hogg. 2014. S100A9 has a protective role in inflammation-induced skin carcinogenesis. *Int. J. Cancer.* 135:798–808. http://dx.doi.org/10.1002/ijc.28725

Nagaraj, S., J.I. Youn, and D.I. Gabrilovich. 2013. Reciprocal relationship between myeloid-derived suppressor cells and T cells. *J. Immunol.* 191:17–23. http://dx.doi.org/10.4049/jimmunol.1300654

Newcomb, D.C., W. Zhou, M.L. Moore, K. Goleniewska, G.K. Hershey, J.K. Kolls, and R.S. Peebles Jr. 2009. A functional IL-13 receptor is expressed on polarized murine $CD4^+$ Th17 cells and IL-13 signaling attenuates Th17 cytokine production. *J. Immunol.* 182:5317–5321. http://dx.doi.org/10.4049/jimmunol.0803868

Ortiz, M.L., L. Lu, I. Ramachandran, and D.I. Gabrilovich. 2014. Myeloid-derived suppressor cells in the development of lung cancer. *Cancer*

Immunol. Res. 2:50–58. http://dx.doi.org/10.1158/2326-6066.CIR-13-0129

Peranzoni, E., S. Zilio, I. Marigo, L. Dolcetti, P. Zanovello, S. Mandruzzato, and V. Bronte. 2010. Myeloid-derived suppressor cell heterogeneity and subset definition. *Curr. Opin. Immunol.* 22:238–244. http://dx.doi.org/10.1016/j.coi.2010.01.021

Schlecker, E., A. Stojanovic, C. Eisen, C. Quack, C.S. Falk, V. Umansky, and A. Cerwenka. 2012. Tumor-infiltrating monocytic myeloid-derived suppressor cells mediate CCR5-dependent recruitment of regulatory T cells favoring tumor growth. *J. Immunol.* 189:5602–5611. http://dx.doi.org/10.4049/jimmunol.1201018

Schmid, M.C., and J.A. Varner. 2012. Myeloid cells in tumor inflammation. *Vasc. Cell.* 4:14. http://dx.doi.org/10.1186/2045-824X-4-14

Shimizu, K., P. Libby, V.Z. Rocha, E.J. Folco, R. Shubiki, N. Grabie, S. Jang, A.H. Lichtman, A. Shimizu, N. Hogg, et al. 2011. Loss of myeloid related protein-8/14 exacerbates cardiac allograft rejection. *Circulation.* 124:2920–2932. http://dx.doi.org/10.1161/CIRCULATIONAHA.110.009910

Sica, A., and V. Bronte. 2007. Altered macrophage differentiation and immune dysfunction in tumor development. *J. Clin. Invest.* 117:1155–1166. http://dx.doi.org/10.1172/JCI31422

Sinha, P., C. Okoro, D. Foell, H.H. Freeze, S. Ostrand-Rosenberg, and G. Srikrishna. 2008. Proinflammatory S100 proteins regulate the accumulation of myeloid-derived suppressor cells. *J. Immunol.* 181:4666–4675. http://dx.doi.org/10.4049/jimmunol.181.7.4666

Sorenson, B.S., A. Khammanivong, B.D. Guenther, K.F. Ross, and M.C. Herzberg. 2012. IL-1 receptor regulates S100A8/A9-dependent keratinocyte resistance to bacterial invasion. *Mucosal Immunol.* 5:66–75. http://dx.doi.org/10.1038/mi.2011.48

Srivastava, M.K., Å. Andersson, L. Zhu, M. Harris-White, J.M. Lee, S. Dubinett, and S. Sharma. 2012. Myeloid suppressor cells and immune modulation in lung cancer. *Immunotherapy.* 4:291–304. http://dx.doi.org/10.2217/imt.11.178

Talmadge, J.E., and D.I. Gabrilovich. 2013. History of myeloid-derived suppressor cells. *Nat. Rev. Cancer.* 13:739–752. http://dx.doi.org/10.1038/nrc3581

Tepper, R.I., D.A. Levinson, B.Z. Stanger, J. Campos-Torres, A.K. Abbas, and P. Leder. 1990. IL-4 induces allergic-like inflammatory disease and alters T cell development in transgenic mice. *Cell.* 62:457–467. http://dx.doi.org/10.1016/0092-8674(90)90011-3

Wang, L., T. Yi, W. Zhang, D.M. Pardoll, and H. Yu. 2010. IL-17 enhances tumor development in carcinogen-induced skin cancer. *Cancer Res.* 70:10112–10120. http://dx.doi.org/10.1158/0008-5472.CAN-10-0775

Xiao, M., C. Wang, J. Zhang, Z. Li, X. Zhao, and Z. Qin. 2009. IFNγ promotes papilloma development by up-regulating Th17-associated inflammation. *Cancer Res.* 69:2010–2017. http://dx.doi.org/10.1158/0008-5472.CAN-08-3479

Youn, J.-I., M. Collazo, I.N. Shalova, S.K. Biswas, and D.I. Gabrilovich. 2012. Characterization of the nature of granulocytic myeloid-derived suppressor cells in tumor-bearing mice. *J. Leukoc. Biol.* 91:167–181. http://dx.doi.org/10.1189/jlb.0311177

Zhao, F., B. Hoechst, A. Duffy, J. Gamrekelashvili, S. Fioravanti, M.P. Manns, T.F. Greten, and F. Korangy. 2012. S100A9 a new marker for monocytic human myeloid-derived suppressor cells. *Immunology.* 136:176–183. http://dx.doi.org/10.1111/j.1365-2567.2012.03566.x